HEAT AND FLUID FLOW MODELING IN TWIN-WIRE WELDING

Meenakshi Devi Parre

A Thesis Submitted to
Indian Institute of Technology Hyderabad
In Partial Fulfillment of the Requirements for
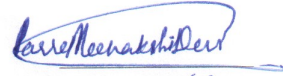The Degree of Master of Technology

भारतीय प्रौद्योगिकी संस्थान हैदराबाद
Indian Institute of Technology Hyderabad

Department of Mechanical Engineering

July 2011

Declaration

I declare that this written submission represents my ideas in my own words, and where ideas or words of others have been included, I have adequately cited and referenced the original sources. I also declare that I have adhered to all principles of academic honesty and integrity and have not misrepresented or fabricated or falsified any idea/data/fact/source in my submission. I understand that any violation of the above will be a cause for disciplinary action by the Institute and can also evoke penal action from the sources that have thus not been properly cited, or from whom proper permission has not been taken when needed.
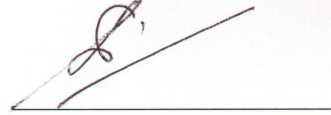
(Signature)

(Meenakshi Devi Parre)

ME09G007
(Roll No.)

Approval Sheet

This thesis entitled 'HEAT AND FLUID FLOW MODELING IN TWIN-WIRE WELDING' by Meenakshi Devi Parre is approved for the degree of Master of Technology from IIT Hyderabad.
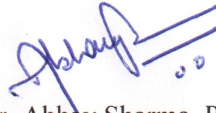
Dr. Saptarshi Majumdar (Ext. Examiner)

Dept. of Chem. Engg. , IITH
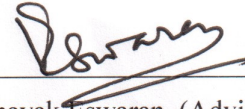
Dr. S.Surya Kumar (Int. Examiner)

Dept. of Mech. Engg. , IITH

Dr. Abhay Sharma, Prof. Vinayak Eswaran (Adviser (s))

Dept. of Mech. Engg. , IITH

Dr. Kirti Chandra Sahu (Chairman)

Dept. of Chem. Engg. , IITH

Acknowledgements

Dedication

To The Almighty

Abstract

Twin-wire welding is a metal joining process that uses two electrodes to generate localized heat at the weld joint. Due to the effect of magnetic arc blow, both of the arcs direct towards each other and subsequently act as a single heat source. This heat source is basically a double-ellipsoidal moving heat source that follows Gaussian distribution. It causes melting of the specimen and formation of weld-pool. Numerical simulation of this entire phenomenon is a classical problem based on Gaussian distributed double-ellipsoidal moving heat source with fluid flow driven by Electro Magnetic Force (EMF), buoyancy, surface tension, marangoni stress and gravity.

Three-dimensional physical model of the specimen is modeled using ANSYS-WORKBENCH environment. This model is imported into commercial Computational Fluid Dynamics (CFD) solver ANSYS-FLUENT 12.0.1, which is based on Finite Volume Method (FVM) of discretization to solve the governing equations, initial and boundary conditions.

The present work aims at developing the heat and fluid flow model for twin-wire welding process over the previous work based on steady state heat conduction alone. It investigates the effectiveness of previous model and suggests suitable modification in flux compensation factor that accounts for cooling time. This work correlates the process parameters like wire- diameter, current and polarity with temperature distribution of the specimen, velocity of the flow in the weld pool and cooling time of the specimen.

Key words: Twin-wire welding, double ellipsoidal heat source, heat and fluid flow modeling, flux compensation factor.

Contents

List of Figures

List of Tables

Chapter 1

Introduction

1.1   Preamble

Welding is a conventional manufacturing technique that is used in joining or fabricating materials, usually metals or thermoplastics, by using heat or pressure or both. The stages involved in this process are, melting the workpieces and adding a filler material to form a pool of molten material i.e. the weld pool, which further cools to become a strong joint. During the various stages of welding process the defects like cracks, distortion, gas inclusions, lack of fusion, incomplete penetration, lamellar tearing, undercutting, residual stresses, reduced strength etc. are observed in and around a welded joint. These defects result directly from the thermal cycle caused by the intense heat input during welding. Hence, in this scenario, the need for studies on heat and fluid flow modeling is pronounced.

1.2   State of the Art

In general, experimentation is done to study the system with the objective to predict how a system will perform under certain set of conditions. It may be infeasible to experiment with a system while it is in hypothetical state or the required outputs are in such a large quantity that frequent experimenting is not possible. Moreover, experimentation may be costly for certain systems. Due to the above reasons, *Modeling* has emerged as one of the important tool for studying and understanding systems. It plays an important role in mechanical systems because of the following facts:

1. Analytical techniques using the mathematical reasoning are used to understand the systems because the mechanisms of mechanical systems are not always easy to understand. Only certain forms of mathematical equations can be solved in practice. Behavior of the system can be approximately estimated by modeling, which could not be otherwise estimated with analytical techniques.

2. Analytical studies cannot always fully accommodate actual set of conditions. Modeling provides flexibility of incorporating such conditions with certain approximations.

3. Systems sometimes act as a black box, in which input and output are known, but what actually is happening inside the system remains unknown. In such cases modeling provides an analogous

environment to predict the behavior of the system.

4. In some studies, it may not be possible to repeat the experiments number of times because of time and cost constraints. In such situations, speed and cost effectiveness of modeling become important.

The complex phenomenon that occurs during welding can be understood from theoretical investigation by mathematical modeling. Modeling of weld pool fluid flow is a typical problem of moving boundary that involves melting and solidification. It is inherently difficult, because the location of solid-liquid interface is not known a priori and must be obtained as a part of solution. The governing equations are non-linear and exact analytical solutions can be obtained only for a limited number of ideal cases. Therefore, considerable interest has been directed towards the use of numerical methods to obtain time dependent solutions for theoretical models that described the welding process.

In 1930s, Rosenthal [1] applied the basic theory of heat flow developed by Fourier to moving heat source which is still the most popular analytical method to calculate the thermal history of welds. As many researchers have shown, Rosenthal's analysis (which assumes a point, a line, or plane source of heat) is subjected to serious errors for temperatures in or near the fusion and heat-affected zones. Rosenthal's solution can give quite accurate results in the regions of work-piece where the temperature is less than 20 percent of melting point. In the Rosenthal's model, error is increased as the heat source is approached because of the infinite temperature at heat source and the thermal properties of material are assumed to be temperature independent. Several researchers have used distributed heat source and different numerical techniques to analyze heat flow in welds, to over come these limitations. John Goldak et al. [2] used Finite Element Modeling(FEM) with double ellipsoidal heat source for 2D analysis where as Robert et al. [3] used semi-discrete technique with hemispherical heat source for 3D analysis. A 3D analytical model for moving heat source has been developed by Nguyen et al. [4] . A completely general 3-D model of the welding process, incorporating the moving heat source and the details of weld pool circulation is still under development. Attempts have also been made to model process variants in Twin-wire welding [5, 6].

1.3   Objective of Study

In the modeling of welding process, simulating the thermal input from the arc to the work-piece and fluid flow in the work-piece are the most important issues. The interaction of a heat source (arc, electron beam and laser) with a weld pool and fluid flow within the weld pool is a complex phenomenon and still cannot be modeled rigorously. A limited literature is available on the distribution of pressure from the heat source, the precise effects of surface tension, buoyancy force and molten metal viscosity.

However, it is known that these factors combine to cause weld pool distortion and considerable stirring. Heat input is effectively distributed throughout the volume of work-piece because of these stirring and digging actions. Heat input and fluid flow are to be modeled and simulated in a coupled manner during the heat and fluid-flow analysis of welding. After developing heat source model and fluid flow model, it can be solved using a numerical technique like Finite volume method (FVM).

- The present work is intended to model and simulate a 3-D transient heat transfer and fluid flow phenomenon on Twin-wire welding using finite volume method.

- It intends to understand the effect of process parameters like current, polarity and wire diameters using different heat inputs on heat transfer and fluid flow with respect to time and fluid flow pattern.

1.4   Thesis Organization

- The following chapter titled 'Literature review' describes the basic concept of heat transfer and fluid-flow with reference to welding and the historical background in this field.

- The chapter titled 'Moving heat source with fluid-flow problem' describes mathematical background for the development of the model which includes governing equations and boundary conditions. Solution algorithm and implementation of User-defined functions have been explained in this chapter. Validation of the model with experimental results has been illustrated in this chapter.

- The chapter titled 'Results and discussion' presents the results and discussion on temperature distribution, fluid flow pattern, influence of polarity, current and wire-diameter on weldment has been carried out.

- Finally this report is concluded in chapter titled 'Conclusions' with the recommendations for future work.

Chapter 2

Literature Review

Since past 70 years the study of heat and fluid flow in weldment are going on. During 1930 to 1940, Rosenthal [1] did the most significant early work. His study is on the analysis of the heat conduction pattern in the work-piece under the influence of moving heat source. This analysis was limited to quasi-stationary state and it considered heat source as a point source. After the pioneering work of Rosenthal [1], many researchers directed their interests in the thermal aspects of welding and later the fluid flow studies were developed gradually. This chapter gives a review of the works carried out in the field of welding.

2.1   Introduction

There are two main classifications of the work carried out in the field of welding process modeling. The first-one deals with experimental and analytical work and the second one deals with numerical methods, such as Finite Element Method (FEM), Finite Difference Method (FDM) and Finite Volume Method (FVM). Literature covering the numerical methods is briefly reviewed in the later part of this chapter. During the period of 1930 to 1970, most of the intense analytical work on this subject was undertaken. After this, the solutions based on the numerical methods predominated. Before analyzing the past work it would be beneficial to discuss some of the basic concepts regarding heat transfer in the welding and twin-wire welding system.

2.2   Heating Phenomenon in Welding

The sources of heat generated during arc welding processes are as follows:

1. Heat generated by the electrical power of the welding arc, this energy input is commonly expressed in terms of heat input per unit length Q as shown in Eqn.2.1.

$$Q = \frac{V.I}{s}, Joule/mm \tag{2.1}$$

where:
V = arc voltage in Volts,

I = arc current in Amperes,

s = travel speed of welding arc in $mmsec^{-1}$.

2. Heat caused by chemical reactions which take place in the electrode coatings, arc atmosphere and molten pool.

3. Heat caused by metal transformation.

The portion of the work-piece immediately under the arc is subjected to the most of the heat transferred by the welding arc. The heat then spreads into further portions of the work-piece. The net heat transferred to the work piece can be stated as shown in the Eqn.2.2.

$$Q_p = \eta VI, \, Watts. \tag{2.2}$$

where η = arc efficiency.

Heat flow in arc welding involves three stages:

1. Heat saturation stage during which the temperature around the heat source is rising.

2. Quasi-stationary stage in which the temperature distribution is stationary in a coordinate system which moves with the heat source.

3. Leveling off stage in which the temperature evens out after the welding arc is extinguished.

The mathematical analysis is simple in the quasi-stationary state, since the problem can be treated as a steady state problem for a moving coordinate system. The quasi-stationary state occurs in a small area close to the weld during long weld cycle. Most of the mathematical analysis conducted on heat and fluid flow in weldments had been done in the quasi-stationary state. Even if the weld is made on considerable length, the areas as mentioned from stage 1 to stage 3 of a weld, heat flow is in non-stationary state. Quasi-stationary state is never reached when the weld is made over a short length and the metal adjacent to a short bead cool much faster than those adjacent to a long weld. Mathematical analysis in the non-stationary state is much more complicated than that in the quasi-stationary state.

Heat flow analysis and fluid flow analysis are the processes of evaluation of temperature pattern and fluid-flow pattern at different points on the surface as well as inside the body of work-piece. Fig. 2.1 shows schematically the temperature distribution in a plate when the heat source is moving at speed s. Dotted curves represent isotherms on the surface. The origin is on the surface, the Y-axis lies in the direction of welding and Z-axis is placed in the thickness of the plate downward. Fourier equation is the fundamental heat equation used for heat transfer analysis. The energy balance equation can be mathematically stated as shown in Eqns.2.3 and 2.4:

$$\nabla.(k\nabla T)) + Q_g = \rho.C_p \frac{DT}{Dt} \tag{2.3}$$

$$\rho.C_p \frac{DT}{Dt} = \frac{DH}{Dt} \tag{2.4}$$

5

where:

Q_g = Heat generation rate in $Jm^{-3}\ sec^{-1}$

k = Thermal conductivity of the work-piece in W/mK

T = Temperature in K

ρ = Density in kg/m^3

C_p= Specific heat at constant pressure in J/kgK

t = time in seconds.
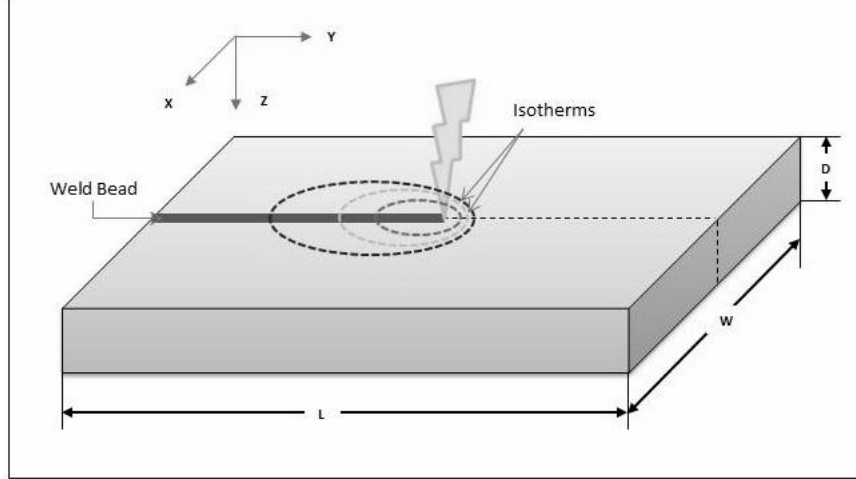
Figure 2.1: Schematic figure showing the temperature isotherms in a plate

Fig. 2.1 shows the temperature contours that are formed on the work-piece on the application of heat by the arc. Heat flow analysis in weldments concentrates on solving Eqn.2.3 of heat conduction for a given initial and boundary conditions with source terms. The boundary conditions are the conditions of heat dissipation at the boundary surface of the structure. Homogeneous Neumann boundary conditions are attributed to all the surfaces in the analysis except the top surface. Initially, the work-piece is at room temperature (isothermal boundary condition) and there is no fluid flow at this state. The temperature of the surrounding medium is the ambient temperature. This is the initial condition. On application of heat, when the temperature of the work-piece rises above the liquidus temperature of the material fluid flow comes into picture. During this process there will be heat loss to the surrounding medium from the work-piece by convection and radiation. The heat loss is represented by laws of convection and radiation as shown in Eqns.2.5 and 2.6.

Law of heat transfer by convection:

$$Q_c = h_c(T_{x,y,z,t} - T_0) \tag{2.5}$$

Law of heat transfer by radiation:

$$Q_r = \varepsilon C_0(T^4_{x,y,z,t} - T^4_0) \tag{2.6}$$

where:

h_c = heat transfer coefficient in W/m^2K.

C_0 $\quad$ = radiation heat transfer coefficient in W/m^2K^4.

$T_{x,y,z,t}$ = temperature of the work-piece in K.

T_0 $\quad$ = ambient temperature in K.

ε $\quad$ = emissivity.

In case of moving source the Cartesian co-ordinate (x, y, z) system is to be transformed into a moving coordinate system (x, ξ, z), where the arc is moving in Y-direction. This coordinate system has center at the arc and it moves with the same speed as that of welding arc as shown in Fig. 2.2.
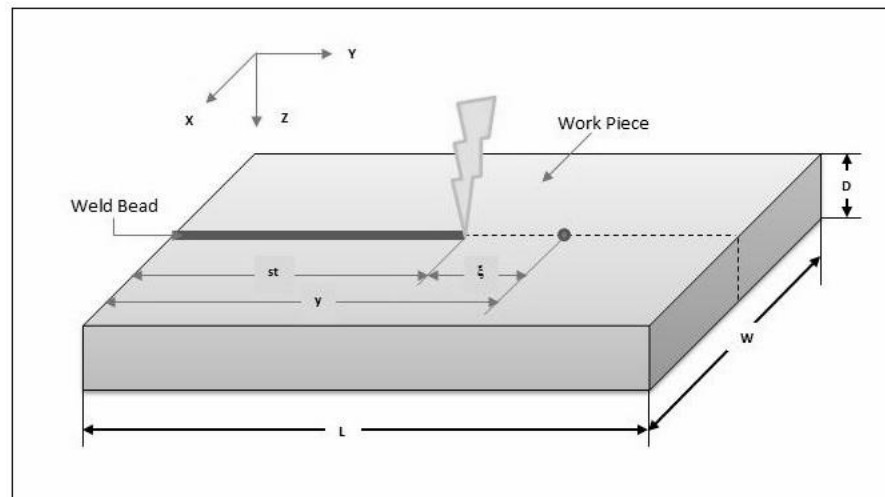
Figure 2.2: Moving Coordinate System

2.3 Models of Heat Flow

Arc is a complex phenomenon and at times it may not be possible to know how the energy generates and distribute from arc to workpiece and how it further influences the fluid flow pattern. The exact distribution of energy from arc can be replaced by some known mathematical functions, which are an approximation to the actual distribution. Such functions are known as heat source models and frequently used to solve the heat transfer problem in welding. Following are the heat source models given by different investigators.

2.3.1 Point Heat Source Model

Rosenthal [1] is the pioneer of analytic solutions of welding. He assumed that heat source can be analogous to a point source and work-piece is analogous to an infinite plane. So, he considered a point source moving relative to an infinite material of workpiece. Point heat source model is used in simulating the surface melt that runs relative to zone that is prone to conduction in welding. This model assumes that the point source moves along the longitudinal direction of the specimen and it is finite in depth and width directions. Even though this model is simple, the main set-back in this model is the region upto which it is confined and it does not define the entire area that is heat-prone.

2.3.2 Line Heat Source Model

At a later stage Rosenthal assumed that heat source is a line perpendicular to the top and bottom surfaces which is in the depth direction [7]. The major problem with point and line source models is that they lead to infinite temperatures at the source. Rosenthal devised an approximate formula using these solutions for predicting the cooling rate and time for a different thicknesses, temperatures and welding conditions of steel. Swift-Hook and Gick [8] approximated Rosenthals solution for different speeds and estimated that the fraction of power required to melt the specimen behaves as a function of the incident power.

Bunting and Cornfield [9] devised a solution in which heat source model is in the form of a cylindrical beam. They obtained this by integrating the line source solution over a circular area. This model is most suitable for laser welding. They found that depending on the diameter of the jet the efficiency of the cutting process could be maximized for a certain power density. Their results were slightly different from experimental results, but they are better than the previous works. ONeill and Steen [10] presented a review of mathematical models of laser cutting of steels.

2.3.3 Surface Heat Source Models

This model distributes the heat input over the surface area. In the disc model proposed by Pavelic et.al. [11], the thermal flux has a Gaussian distribution along the Z-Z plane as shown in Fig. 2.3. The mathematical expression for this model is as follows:

$$q(r) = q(0)e^{-Cr^2} \tag{2.7}$$

where:

$q(r)$ = surface flux at radius r (W/m^2)

$q(0)$ = maximum flux at the center of the heat source (W/m^2)

C = distribution width coefficient (m^{-2})

r = radial distance from the center of the heat source (m)

A simple physical meaning can be associated with 'C'. If a uniform flux of magnitude $q(r)$ is distributed in a circle of diameter d= $2/\sqrt{C}$, the rate of energy input would be ηVI, i.e., the circle would receive exactly the same amount of energy from the arc. Therefore the coefficient, 'C' is related to the source width as shown in Fig. 2.4 a more concentrated source would have a smaller diameter and a larger value of 'C'.

If it is assumed that arc acts on a circular area with diameter DH (hot spot dia.) $= 2r_h$ and in accordance with reference [10] $q_{min} = 0.05q_{max}$ at the outer periphery, then

$$q_{min} = q(0).e^{Cr_h^2} \tag{2.8}$$

but

$$q_{min} = 0.05.q_{max} \tag{2.9}$$

from Eqn. (2.8) and (2.9)

$$C = \frac{ln20}{r_h^2} \tag{2.10}$$

8
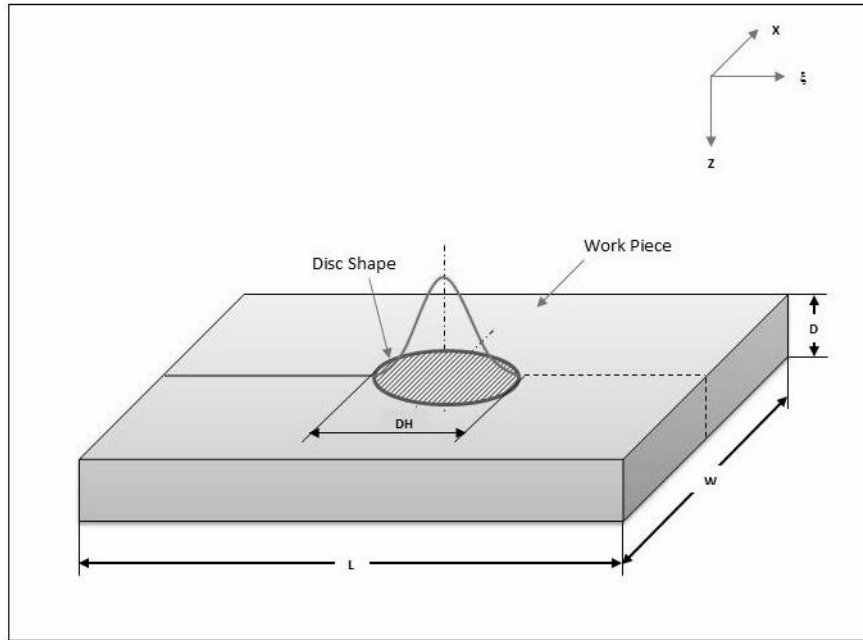
Figure 2.3: Palvelic or disc model
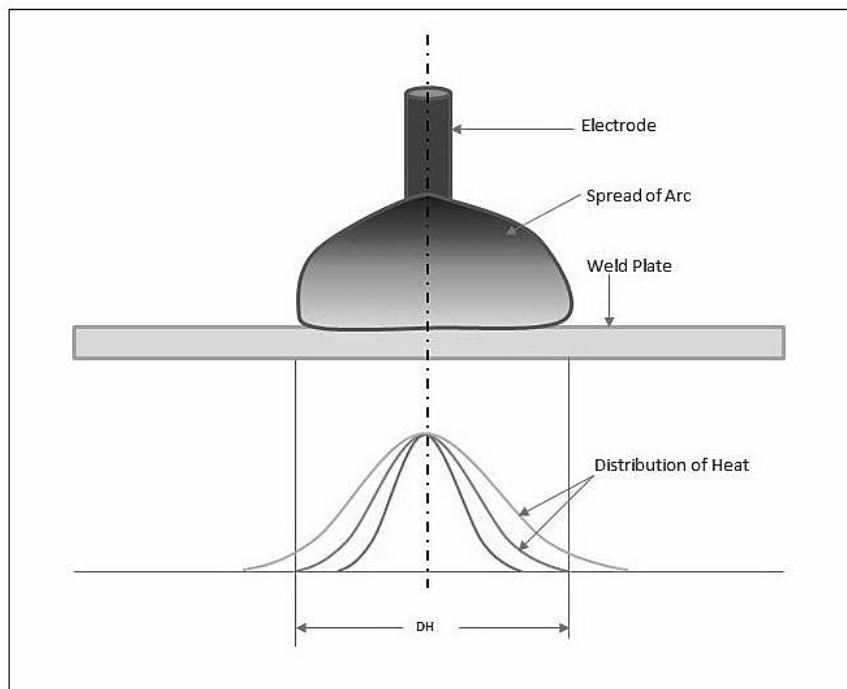
Figure 2.4: Radial distribution of heat source density

Friedman [12] suggested an alternative from the Pavelic 'disc' model, based on this and expressed this equation in a moving coordinate system for 2-D case.

The mathematical expression for Friedman model is as follows:

$$Q_g(x, \xi) = \frac{3Q_p}{\pi r_h^2} e^{\left(\frac{-3x^2}{r_h^2}\right)} e^{\left(\frac{-3\xi^2}{r_h^2}\right)} \tag{2.11}$$

It is convenient to express the Eqn. 2.11 in a coordinate system fixed to the work piece. Additionally, a lag factor 'τ' is needed to define the position of source at time t =0. The transformation relating the fixed and moving coordinate system is shown in Eqn.2.12:

$$\xi = y + s(\tau - t) \tag{2.12}$$

2.3.4 Volume Heat Source Models

When the effective depth of penetration in welding is small, the surface heat source model like Pavelic has been successful. However, for sources with high power density, digging action of the arc had been ignored. In such cases a volume source based on Gaussian distribution is prescribed [2]. Different volume heat sources are discussed in the following section.

a. Hemispherical Power Density Source Model

The first volumetric heat source model is the Hemispherical power density source model. It considers uniform distribution of heat within a hemisphere having diameter DH, as shown in Fig. 2.5. This distribution can be stated in a moving coordinate system:

$$Q_g(x, \xi, z) = \frac{3Q_p}{\pi r_h^2} e^{\left(\frac{-3x^2}{r_h^2}\right)} e^{\left(\frac{-3\xi^2}{r_h^2}\right)} e^{\left(\frac{-3z^2}{r_h^2}\right)} \tag{2.13}$$

Hemispherical heat source is expected to model an arc better than a disc model with some limitations. The molten weld pool in many welds is far from being spherical in shape. In case of strip electrodes or deep penetration applications, a hemispherical source is not appropriate for welds because they are not spherically symmetric. In order to remove these constraints, and make the formulation more accurate, an ellipsoidal volume source is prescribed.

b. Ellipsoidal Power Density Source Model

The Gaussian distribution of heat density in an ellipsoid with center at (0,0,0) and semi-axes a, b, c parallel to coordinate axes x, ξ, z are given by Eqn.2.14:

$$Q_g(x, \xi, z) = Q(0)e^{-Ax^2}e^{-B\xi^2}e^{-Cz^2} \tag{2.14}$$

$$\int_{-\infty}^{\infty}\int_{-\infty}^{\infty}\int_{-\infty}^{\infty} Q_g \, \mathrm{d}x d\xi dz = 2.\eta.V.I \tag{2.15}$$

$$2.\eta.V.I = 8. \int_{0}^{\infty}\int_{0}^{\infty}\int_{0}^{\infty} Q_g(0)e^{-Ax^2}e^{-B\xi^2}e^{-Cz^2} \, \mathrm{d}x d\xi dz \tag{2.16}$$

On solving the Eqns.2.16 and 2.2 we get:

$$2.Q_p = Q_g(0)\frac{\pi\sqrt{\pi}}{\sqrt{A.B.C}} \tag{2.17}$$
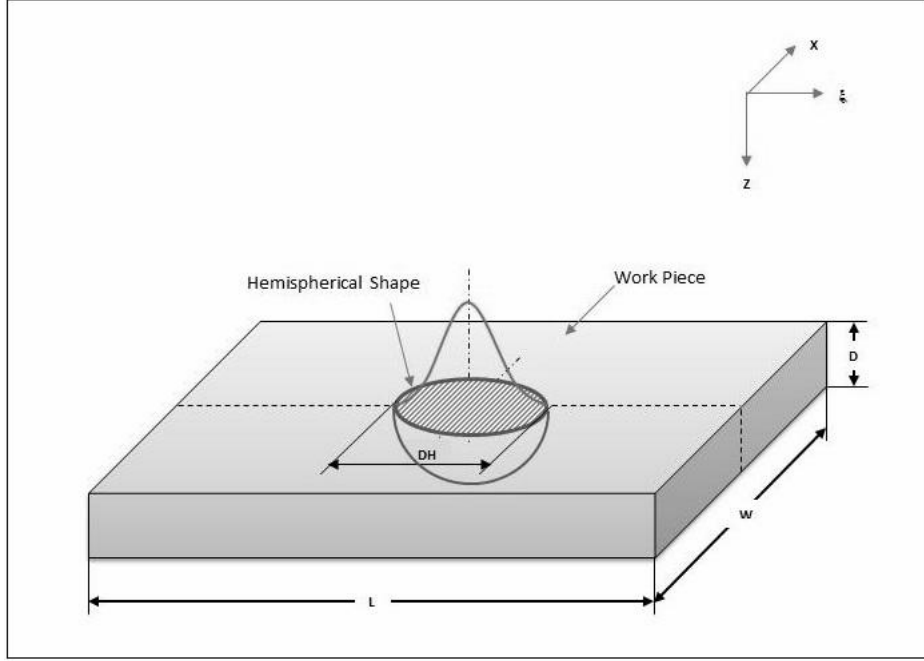
Figure 2.5: Hemispherical distribution of heat source density

or

$$Q_g(0) = 2.Q_p \frac{\sqrt{A.B.C}}{\pi\sqrt{\pi}} \qquad (2.18)$$

To evaluate a, b, c the semi axes of ellipsoid in the respective directions are defined such that the heat density falls to $0.05\ Q_g(0)$ at the surface of the ellipsoid. In x-direction:

$$Q_g(a,0,0) = Q_g(0)\, e^{-Aa^2} = 0.05 Q_g(0) \qquad (2.19)$$

hence

$$A = \frac{ln20}{a^2} \cong \frac{3}{a^2} \qquad (2.20)$$

similarly

$$B = \frac{ln20}{b^2} \cong \frac{3}{b^2} \qquad (2.21)$$

and

$$C = \frac{ln20}{c^2} \cong \frac{3}{c^2} \qquad (2.22)$$

Thus:

$$Q_g = \left(\frac{6\sqrt{3}Q}{\pi\sqrt{\pi}.a.b.c}\right) e^{\frac{-3(x)^2}{a^2}}\, e^{\frac{-3(y-st)^2}{b^2}}\, e^{\frac{-3z^2}{c^2}} \qquad (2.23)$$

c. Double-Ellipsoidal Power Density Source Model

Simulation with the ellipsoidal heat density distribution revealed that the temperature gradient in front of the heat source was not so steep and gentler gradient at the trailing edge of the molten pool was steeper than experimental experience [2]. To overcome this limitation, two ellipsoidal sources are combined as shown in Fig. 2.6.

11
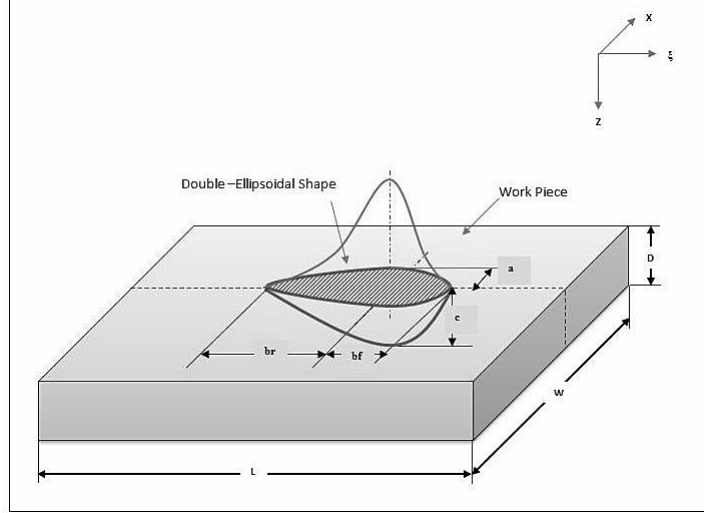
Figure 2.6: Double ellipsoidal distribution of heat source density

The front half is the quadrant of one ellipsoidal source while the rear half is of another, having semi-axis b_f and b_r respectively. In this model, the fractions f_f and f_r of the heat deposited in the front and rear quadrants are needed, where $f_r + f_f = 2$. Heat density in the front and rear becomes as follows:

In front quadrant:

$$Q_g(x,y,z,t) = f_f \left(\frac{6\sqrt{3}Q}{\pi\sqrt{\pi}.a.bf.c} \right) e^{\frac{-3(x)^2}{a^2}} e^{\frac{-3(y-st)^2}{bf^2}} e^{\frac{-3z^2}{c^2}} \tag{2.24}$$

In rear quadrant:

$$Q_g(x,y,z,t) = f_r \left(\frac{6\sqrt{3}Q}{\pi\sqrt{\pi}.a.br.c} \right) e^{\frac{-3(x)^2}{a^2}} e^{\frac{-3(y-st)^2}{br^2}} e^{\frac{-3z^2}{c^2}} \tag{2.25}$$

The parameters a, b, c in Eqn. (2.24) and (2.25), can have different values in the front and rear quadrants. Indeed, in welding dissimilar metals, it may be necessary to use four octants, each with independent values of a, b, c. Double ellipsoidal model of heat distribution is versatile because it can accommodate all the shapes of electrodes. Physically the parameters a, b, c are the radial dimensions of the molten weld pool in front, behind, to the sides and underneath the arc. Christensen [13] defined a non-dimensional operating parameter and non-dimensional coordinate system, which have been discussed in the forth-coming part, regarding these parameters.

2.4 Models of Fluid Flow

Fluid flow during the melting is governed by different forces including gravity, surface tension, electromagnetic force etc. The processes like Submerged Arc Welding (SAW) employs high currents. So, the electromagnetic or Lorentz force in the moving cavity of weld pool transport liquid to the rear of the cavity as shown in Fig. 2.7. The Electro Magnetic Force (EMF) is the dominant force for driving the fluid flow [14]. Fig. 2.7 depicts the generally accepted flow pattern in submerged arc welding. The metal that melts at the front half of the weld pool flows in the downward direction and on both the sides of the longitudinal axis. The flow reverses at the rear side of the weld pool.
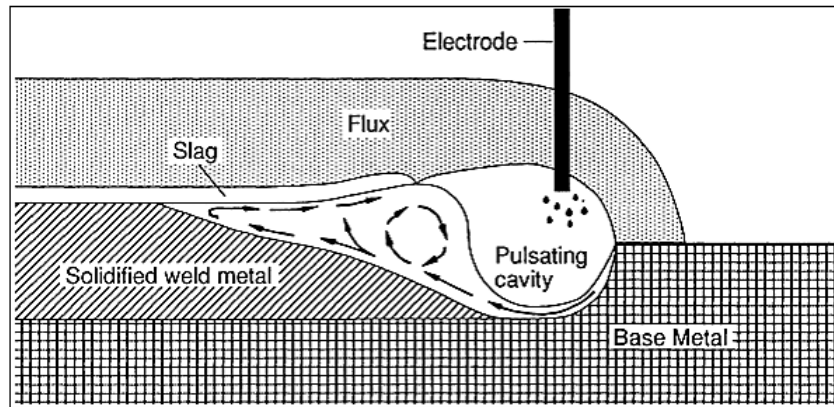
Figure 2.7: Schematic showing typical flow pattern in a submerged arc weld pool.Source: Ref [15]

The problem of fluid flow in welding has been addressed in the following three ways:

2.4.1 Work-piece Based Model of Fluid Flow

Many of the researchers [1-27] considered the heat and fluid flow within the work piece itself without considering the effect of arc and molten metal droplet impingement. These models are considered as work-piece based models because the heat required for melting and flow is assumed to be supplied by a heat source situated within the body of the work-piece. In addition, the effect of arc current and resulting EMF are also simplified by assuming a suitable current distribution.

A Kumar and T Debroy considered [16] work-piece as the domain and developed a numerical model to calculate the current density and magnetic flux fields and the resulting 3D EMF in the entire weldment.

2.4.2 Arc Based Model of Fluid Flow

In this model, arc is separately modeled on the basis of plasma properties. The conservation equations for mass, momentum, energy and current are solved and a mathematical model has been developed to predict the velocity, temperature, and current density distributions in the weldment by Wu et.al [17]. Welding arc and the weld pool surface have been dynamically coupled during the solution of the conservation equations.

Tanaka et al. [18] focussed on the increase in the weld bead penetration depth in stainless steel using the gas tungsten arc (GTA) process by utilizing flux materials like oxides and halides. It has been stated that there is a strong relation between anode roots and the metal vapor phenomenon from the weld pool. This further influences the temperature distribution on the surface of weld pool.

Dong et al. [19] developed a numerical model for heat transfer and fluid flow using a coupled model of the welding arc and weld pool. This model has not used the empirical Gaussian boundary conditions and instead of that it used reliable boundary conditions for weld pool analysis. A two-dimensional axisymmetric numerical model of the argon arc has been developed.

13

2.4.3   Unified Model of Fluid Flow

In this category, the arc and work-piece are modeled as a single entity. In addition, the mass transfer from the consumable electrode is also incorporated in the model.

Wang et. al [20] developed a mathematical model to simulate the dynamic impinging process of filler droplets onto the weld pool in spot gas metal arc welding (GMAW). Filler droplets periodically impinge onto the specimen which results in the formation of weld pool.

Tanaka et al. [21] developed a numerical model for balances of mass, energy, and force in the welding phenomena to clarify the formative mechanism of weld penetration in an arc welding process. A unified numerical model, which shows an interaction between the arc plasma and the weld pool has been developed. Fan and Kovacevic [22] developed a theoretical model which shows the globular transfer in GMAW. In a single unified model, the heat and mass transfer in the electrode, arc plasma and molten pool are considered. The transport phenomena are dynamically studied using the volume of fluid method in the processes like formation of droplet and detachment, droplet flight in arc plasma, impingement of droplets on the molten pool and solidification after the arc extinguishes.

The models described above are numerically solved. The following section gives a brief description based on numerical techniques.

2.5   Numerical Techniques

Several investigators used numerical techniques using Finite Difference Method, Finite Element Method and Finite Volume Methods of discretization with the advent of high-speed computers. These computers are used to solve the governing equations along with the boundary conditions within the specified domain. In fact, numerical techniques are more preferable for irregular geometries than analytical techniques because of less complexity. Macqueene et. al [23] reviewed the numerical methods applied to welding related problems as given in the following section.

2.5.1   Finite Difference Method (FDM).

In FDM, the derivatives of governing equations are replaced by algebraic difference quotients. The dependent variables in the governing equations can be obtained by solving the system of algebraic equations at discrete grid points [24]. Enlisted below are some of the investigations to analyze the heat and fluid flow in the weldment using FDM.

Pavelic et al. [25] used a Finite Difference Method to determine the temperature distribution in a 2-D plate with line heat source. The shape of the melt pool was correlated with welding variables, and this isotherm was used as a boundary conditions. Thus in this work boundary condition was evaluated with experiment. Better agreement of peak temperatures was found between the analytical and experimental work.

Robert L. et al. [3] developed a new technique for 3-D transient heat transfer computations of autogeneous arc welding. The heat equation was solved using an efficient semi-discrete technique using a combination of unequally spaced grids concentrated near the arc in order to minimize the total number of nodes. Finite difference was used for the spatial terms and the resulting ordinary equation for the transient temperature was solved by Runge-Kutta technique. They used tempera-

ture dependent thermal properties and computed temperature profiles in ideal conditions as well as variations due to defects.

2.5.2 Finite Element Method (FEM).

In FEM, a structure is basically considered as an assembly of finite elements whose displacement is a function of position. FEM uses interpolation and weighted integration to obtain the solution variables [24]. Enlisted below are some of the investigations into the heat and fluid flow in the weldment using FEM.

Friedman and Glickstien [12] used a FEM analysis for transient heat conduction to investigate the effect of a number of welding parameters, including the magnitude of heat input from the arc, the distribution of heat input over the surface of the weldment and duration of the heat input on the thermal characteristics - in particular the weld bead shape and depth of penetration. They demonstrated the potential for calculating the optimum combination of welding parameters for a given weld joint.

Kurtz and Segerlind [26] used a non-linear finite element model to optimize the welding parameters for weld joint strength when a certain desired metallurgical structure is achieved.

Goldak et al. [2] developed a mathematical model for weld heat source based on a Gaussian distribution of the power density. They developed a non-linear, transient FEM heat-flow program for thermal stress analysis of welds. They computed the results of temperature distributions for submerged arc welds in thick plate and compared them with the experimental values of Christensen et al. [13].

Tekriwal and Mazumdar [27] developed a 3-D transient heat conduction model for arc welding using FEM software ABAQUS. They compared the numerically predicated size of the melt pool and the HAZ with the experimental results obtained by United States Army Construction Research Laboratory and found good Agreement.

Bonifaz [28] considered a 2-D FEM based model, which used thermal efficiency to quantify the energy, made available by the arc. He used FEM code COSMOS, produced by Structural Research and Analysis Corporation and compared his results with experimental work of Christensen et al.[13] and the other models that of Kurtz et al. [26] and Goldak et al. [2].

Silva Prasad and Narayanan [29] developed a 3-D FEM based model using a transient adaptive grid technique. It gives a finer mesh around the arc source, where temperature gradient is high, and a coarse mesh in other places. This way, both the accuracy and computational efficiency of the analysis can be increased.

2.5.3 Finite Volume Method (FVM).

In FVM, the integral form of governing equations are considered to solve for the solution variables. This numerical technique is more convenient for the models where the domain is complex.[24]. Enlisted below are some of the investigations into the heat and fluid flow in the weldment using Finite Volume Method(FVM).

L.Han and F.W. Liou [30] developed a mathematical model to simulate the material interaction in Laser welding. Melting, solidification and evolution of the free surface are incorporated in the present model.

Zhou et. al [31] carried out numerical study to investigate the heat transfer and fluid flow in Laser welding. In the model, the continuum formulation was used to handle solid phase, liquid phase, and mushy zone during melting and solidification processes. In order to understand latent heat enthalpy method was used.

Wang et. al [32] made simulations for calculating the velocity vectors in the laser weld pool. Their study included the effects of buoyancy forces also.

Wang et. al [33] numerically simulated the application of volumetric heat source using control volume based method. Then, the equations of species, mass, momentum and energy are solved.3D hydrodynamic software FLUENT was used for simulation.

Based on the literature review, Finite Volume Method of numerical technique has been chosen to numerically simulate the heat and fluid flow model because of its flexibility for complex domains. Even though the present domain is not complex, FVM has been chosen based on the future scope of work which may require a complex domain. The commercial Computational Fluid Dynamics (CFD) software ANSYS-FLUENT is tool that numerically simulates the governing equations of the model using FVM. So, this software is considered for solving the problem of heat and fluid flow in twin-wire welding. The following section describes the twin-wire welding set-up.

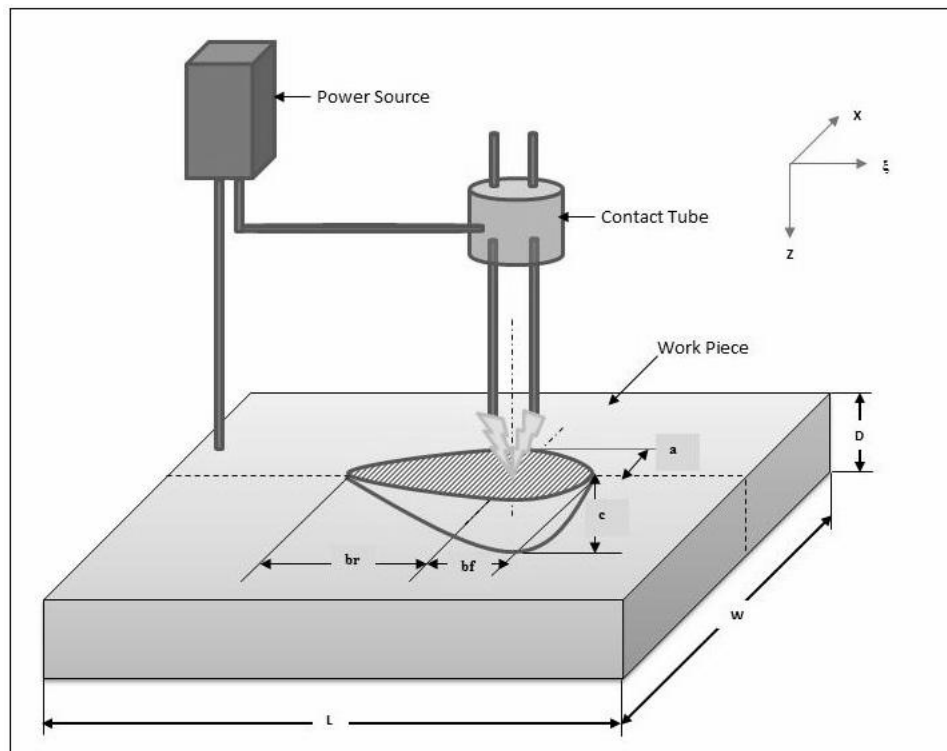## 2.6 Twin-Wire Welding Set-up

Figure 2.8: Twin-wire welding set-up

Twin-wire welding is a type of multiple arc welding system in which two wires are used for the heat source. It is used where the increased deposition rate and higher welding speeds are the requirements. Two electrodes are fed from a single power source through a contact tube as shown in Fig.2.8.

The figure shown above depicts a twin-wire parallel power technique in which two electrodes are fed through a single contact tube. The deposition rate is two times that of a single electrode in this set-up. In twin wire welding, both the arcs pull towards each other because of the back blow at the leading arc and forward blow at the trailing arc as shown in the Fig.2.8. In such a complicated arrangement, heat and fluid flow studies are quite interesting.

2.7 Scope of Present Work

It is evident from the literature review that a number of investigations have been carried out on heat transfer and fluid flow analysis but all of them have taken single moving heat source. Analytically as well as numerically, numbers of investigations have been successfully carried out for a single heat source. In one of the previous work [5], heat source for twin-wire welding has been proposed on the basis of stationary heat source. The model parameters have been estimated on the basis of comparison between actual and predicted peak temperature. It is important to note that there has been no work which deals with fluid flow in twin-wire welding. Moreover, the effect of process parameters on fluid flow is still not reported. Thus the present investigation seeks to investigate the fluid flow in twin-wire. The objectives of the present investigation are as follows:

1. Modeling of fluid flow in twin-wire weld pool by numerically solving energy and fluid flow equations.

2. Existing heat source model for twin-wire have been used in solving simple heat conduction problem. The present investigation aims to evaluate the effectiveness of the models and propose necessary modifications.

3. The present investigation seek to understand the effect of process parameters like current, wire-diameter and polarity on various thermal effects like cooling time, flow velocity and peak temperature.

2.8 Statement of Problem

The present investigation aims at modeling and simulating the heat and fluid flow phenomenon in twin-wire welding. The precise effects of flux compensation factor on the cooling rate of the specimen are to be analyzed. This research aims to improve the heat transfer model of twin-wire welding to heat and fluid flow model by considering the driving forces of fluid flow such as electro magnetic force, buoyancy, surface tension, marangoni stresses and gravity.

Chapter 3

Moving Heat Source With Fluid Flow Problem

3.1 Mathematical Background

This section gives the mathematical background to numerically simulate the problem using FVM in ANSYS-FLUENT environment. The heat transferred to the workpiece is double-ellipsoidal heat source that follows gaussian distribution. This is the source term for energy equation. The mathematical equations for fluid flow driven by electromagnetic force, buoyancy force, surface tension, marangoni stresses and gravity are stated and explained. The governing equations of energy and momentum are to be solved in the work-piece domain. They are represented in the following section.

3.1.1 Governing Equations

Governing equations are the mathematical equations that are obtained when the fundamental laws of mechanics are applied to the energy and fluid flow in the domain.

Continuity Equation

$$\frac{\partial(\rho u)}{\partial x} + \frac{\partial(\rho v)}{\partial y} + \frac{\partial(\rho w)}{\partial z} = 0. \tag{3.1}$$

Energy Equation

This is Enthalpy form of energy equation.

$$\frac{\partial H}{\partial t} + \nabla.(sH) = \nabla.(k\nabla T) + Q_g(x, y, z, t) \tag{3.2}$$

where:

$Q_g(x, y, z, t) =$ Source term for energy equation.

It is the total volumetric heat generation rate of the heat source. The source term for energy is taken from [5]. Double ellipsoidal heat source moving in X-direction with the flux compensation factor (ϕ) is represented by Eqns. 3.3 and 3.4.

$$Q_g(x, y, z, t) = \phi f_f \left(\frac{6\sqrt{3}Q}{\pi\sqrt{\pi}.a.b_f.c} \right) e^{\frac{-3(x-st)^2}{b_f^2}} e^{\frac{-3y^2}{a^2}} e^{\frac{-3z^2}{c^2}} \tag{3.3}$$

$$Q_g(x, y, z, t) = \phi f_r \left(\frac{6\sqrt{3}Q}{\pi\sqrt{\pi}.a.b_r.c} \right) e^{\frac{-3(x-st)^2}{b_r^2}} e^{\frac{-3y^2}{a^2}} e^{\frac{-3z^2}{c^2}} \tag{3.4}$$

where:

f_f = Heat input fraction in the front arc.

f_r = Heat input fraction in the rear arc.

In the above equations the variable ϕ represents 'Flux compensation factor' which signifies the fraction of heat available for melting the specimen.

Momentum Equations

These are Navier-Stokes equations:

X-Momentum Equation:

$$\frac{\partial(\rho uu)}{\partial x} + \frac{\partial(\rho uv)}{\partial y} + \frac{\partial(\rho uw)}{\partial z} = -\frac{\partial P}{\partial x} + \frac{\partial}{\partial x}\left(\mu\frac{\partial u}{\partial x}\right) + \frac{\partial}{\partial y}\left(\mu\frac{\partial u}{\partial y}\right) + \frac{\partial}{\partial z}\left(\mu\frac{\partial u}{\partial z}\right) + S_x \tag{3.5}$$

Y-Momentum Equation:

$$\frac{\partial(\rho vu)}{\partial x} + \frac{\partial(\rho vv)}{\partial y} + \frac{\partial(\rho vw)}{\partial z} = -\frac{\partial P}{\partial y} + \frac{\partial}{\partial x}\left(\mu\frac{\partial u}{\partial x}\right) + \frac{\partial}{\partial y}\left(\mu\frac{\partial v}{\partial y}\right) + \frac{\partial}{\partial z}\left(\mu\frac{\partial v}{\partial z}\right) + S_y \tag{3.6}$$

Z-Momentum Equation:

$$\frac{\partial(\rho wu)}{\partial x} + \frac{\partial(\rho wv)}{\partial y} + \frac{\partial(\rho ww)}{\partial z} = -\frac{\partial P}{\partial z} + \frac{\partial}{\partial x}\left(\mu\frac{\partial u}{\partial w}\right) + \frac{\partial}{\partial y}\left(\mu\frac{\partial w}{\partial y}\right) + \frac{\partial}{\partial z}\left(\mu\frac{\partial w}{\partial z}\right) + S_z \tag{3.7}$$

S_x = Source term for X-momentum.

S_y = Source term for Y-momentum.

S_z = Source term for Z-momentum.

The source terms represent the driving forces of fluid flow can be defined as follows:

$S_x = F_x$.

$S_y = F_y$.

$S_z = F_z + F_b$.

Electro-magnetic Force (EMF) is an outcome of interaction between induced magnetic field (B) and current flow (J) in the weldment [16]. Tsao and Wu [34] derived the following expressions for the Electro Magnetic Force (EMF) field which are used as the source terms for EMF in the present research. F_x, F_y and F_z represent the X,Y and Z components of Electro magnetic force. F_b represents

the Buoyancy force. The effects of Marangoni stresses and surface tension are also considered to study the fluid flow. Surface tension and marangoni effect are considered as interfacial forces and not as body forces in this research because the surface of the weld pool is assumed to be flat always. Since the surface tension of the molten metal in the weld pool depends on the temperature of the cell[20], the value of temperature coefficient of surface tension $= -4.3 \times 10^{-4} N/mK$ is taken from [30] to account for surface tension (Marangoni effect).

$$F_x = \frac{-\mu_m I^2}{4\pi^2 \sigma_j^2 r} e^{\frac{-r^2}{2\sigma_j^2}} [1 - e^{\frac{-r^2}{2\sigma_j^2}}] (1 - \frac{Z}{D})^2 \frac{X}{r} \tag{3.8}$$

$$F_y = \frac{-\mu_m I^2}{4\pi^2 \sigma_j^2 r} e^{\frac{-r^2}{2\sigma_j^2}} [1 - e^{\frac{-r^2}{2\sigma_j^2}}] (1 - \frac{Z}{D})^2 \frac{Y}{r} \tag{3.9}$$

$$F_z = \frac{-\mu_m I^2}{4\pi^2 r^2 c} [1 - e^{\frac{-r^2}{2\sigma_j^2}}] (1 - \frac{Z}{D})^2 \tag{3.10}$$

$$F_b = \rho g \beta (T_{(x,y,z,t)} - T_{(0)}) \tag{3.11}$$

where:

μ_m = magnetic permeability of the specimen material in H/m.
I = Current in Amperes.
σ_j = effective radius of the arc in mm.
r = radial distance from the arc location in mm.
D = Thickness of the specimen in mm.
β = thermal expansion coefficient of the specimen material in K^{-1}.

3.1.2 Initial and Boundary conditions

Initial condition: Initially work-piece is at room temperature $T_0 = 27\,^0C$ in the absence of pre-heating. So the initial condition can be stated as follows:

$\quad T_{(x,y,z,0)} = T_0$

Boundary conditions:

The top surface on which heat source is acting is subjected to convection and radiation whereas all the other surfaces are insulated.

Boundary Conditions:

Since the heat source is a moving and the specimen is stationary, the following boundary conditions hold good when the origin of the heat source is at the center of top surface of the specimen.

$\quad$ At $X = \frac{-L}{2}$:
$\quad u = 0$; $v = 0$; $w = 0$; $\frac{\partial H}{\partial X} = 0$ (Homogeneous Neumann Boundary condition).

$\quad$ At $X = \frac{L}{2}$:

$u = 0$; $v = 0$; $w = 0$; $\frac{\partial H}{\partial X} = 0$ (Homogeneous Neumann Boundary condition).

At $Y = \frac{W}{2}$:
$u = 0$; $v = 0$; $w = 0$; $\frac{\partial H}{\partial Y} = 0$ (Homogeneous Neumann Boundary condition).

At $Y = \frac{-W}{2}$:
$u = 0$; $v = 0$; $w = 0$; $\frac{\partial H}{\partial Y} = 0$ (Homogeneous Neumann Boundary condition).

At $Z = D$:
$u = 0$; $v = 0$; $w = 0$; $\frac{\partial H}{\partial Z} = 0$ (Homogeneous Neumann Boundary condition).

At $z = 0$:
$u = 0$; $v = 0$; $w = 0$; $\frac{\partial H}{\partial t} = Q_g(x, y, z, t) - Q_{cr}$

where:

u,v,w are velocity components along X,Y,Z directions respectively. L,W,D are the length, width and depth of the work-piece and Q_{cr} is the heat loss to the atmosphere from the specimen due to both convection and radiation.

3.1.3 Assumptions in the model

The following assumptions have been made while solving the problem numerically:

1. It is assumed that there is no heat loss from all the boundaries of the specimen except the top surface. Previous investigators like Christensen [13], Goldak [2] and Kurtz and Segerlind [26] etc. considered this assumption.

2. It is assumed that, at a given instant, there is no heat loss from the region that is under the arc [29].

3. A combined convection and radiation boundary condition $h = 24.1x10 - 4\ \varepsilon T^{1.61}\ (W/m^2 C)$ has been used on the top surface except under the region that is under the arc. The value of ε=0.82 has been assumed as suggested by Robert L. [3].

4. Temperature dependent thermo-physical properties for low carbon structural steel at elevated temperatures have been taken same as that suggested by M.R. Frewin and D.A. Scott [35].

5. The magnetic permeability of the material is assumed to be constant because the electro-magnetic properties of the specimen are considered to be temperature independent [16].

6. The current density follows Gaussian distribution on the weld-pool [16].

7. Only angular component of the magnetic flux exists and the radial and axial components of the magnetic flux does not exist [16].

8. Along the depth direction, the angular component of magnetic flux and the vertical component of current density decrease linearly and become zero at the bottom surface [34].

9. Surface of the weld pool remains flat always.

3.2 Geometry and Mesh Development

The first step in model development is building the model using ANSYS WORKBENCH environment. This feature is available in ANSYS-FLUENT software package, which provides sophisticated geometric acquisition, mesh generation, wide variety of solver outputs and post-processing. The geometry of 300 mm length, 100 mm width and 22 mm depth was developed in ANSYS-WORKBENCH environment. Meshing has been performed in the same environment. Grid convergence test has been performed by varying the maximum and minimum size of tetrahedron shaped cell. Fig.3.1 and Fig.3.2 show the geometry and mesh developed in ANSYS-WORKBENCH environment.
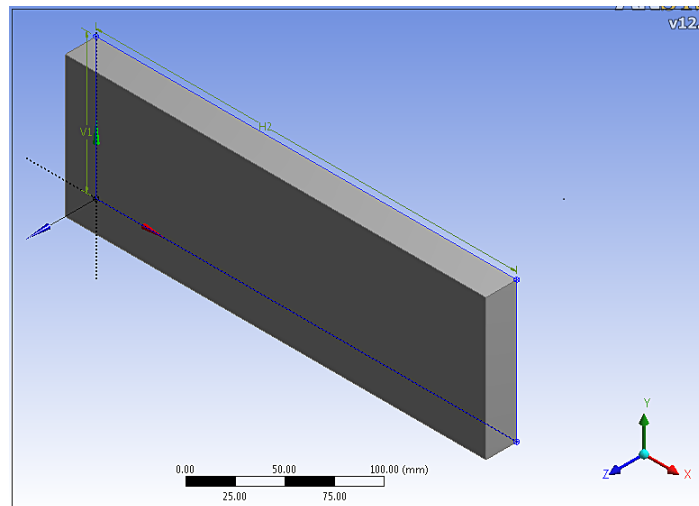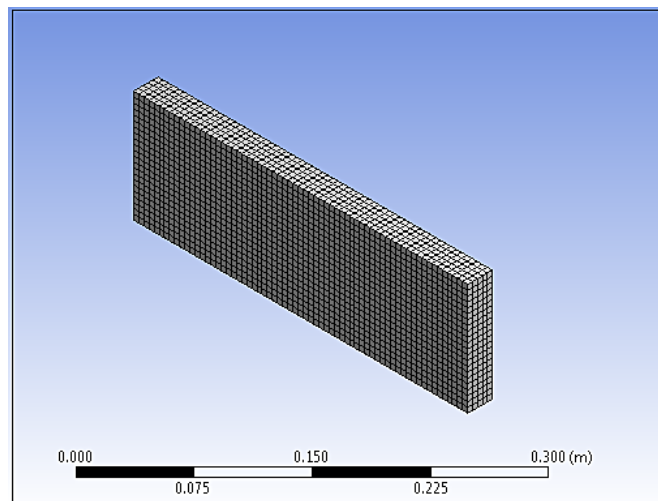

Figure 3.1: Geometry.

Figure 3.2: Mesh.

3.3 Material Properties

The Thermo-Physical properties of work-piece are linearly interpolated for the intermediate temperatures. All Thermo-physical properties are considered to be temperature dependent. Thermal conductivity, specific heat and density were taken from M. R. Frewin and D. A. Scott [35]. These properties are shown in Table 3.1.

Table 3.1: Thermo-Physical properties of the work-piece material

S.No	Temperature (^oC)	Thermal Conductivity (W/m^oK)	Specific Heat (J/Kgm^3)	Density (Kg/m^3)
1	75	51.3	486	7852
2	100	51.1	494	7845
3	175	49.5	519	7824
4	200	49.0	526	7816
5	275	46.8	557	7763
6	300	46.1	566	7740
7	375	43.6	599	7727
8	475	40.2	662	7720
9	500	39.4	684	7711
10	575	36.6	749	7680
11	600	35.6	773	7669
12	675	32.8	846	7636
13	700	31.8	1139	7625
14	730	30.1	1384	7612
15	750	28.9	1191	7602
16	775	27.5	950	7590
17	800	26.0	931	7578
18	1000	27.2	779	7552
19	1500	29.7	400	7268
20	1540	29.7	400	7218
21	1590	29.7	847	7055
22	1840	29.7	847	6757
23	1890	29.7	400	6715
24	2860	29.7	400	5902

3.4 Method of solution

Fig. 3.3 describes the solution process that is implemented for solving the governing equations. In this, the user defined profile for the boundaries is considered at first. At this step, the combined convection and radiation losses that are applied to the top surface (excluding the area under the arc) are attributed to the top surface and homogeneous Neumann boundary condition is applied to all the surfaces other than the top surface.

In order to include the source terms for energy and momentum in the solver, User-defined functions(UDFs) are required to customize the FLUENT code to fit this particular modeling need. Since transient cell zone conditions cannot be defined by the FLUENT graphical user-interface, a UDF is written to apply heat source and driving forces for fluid flow on the work piece. They are defined
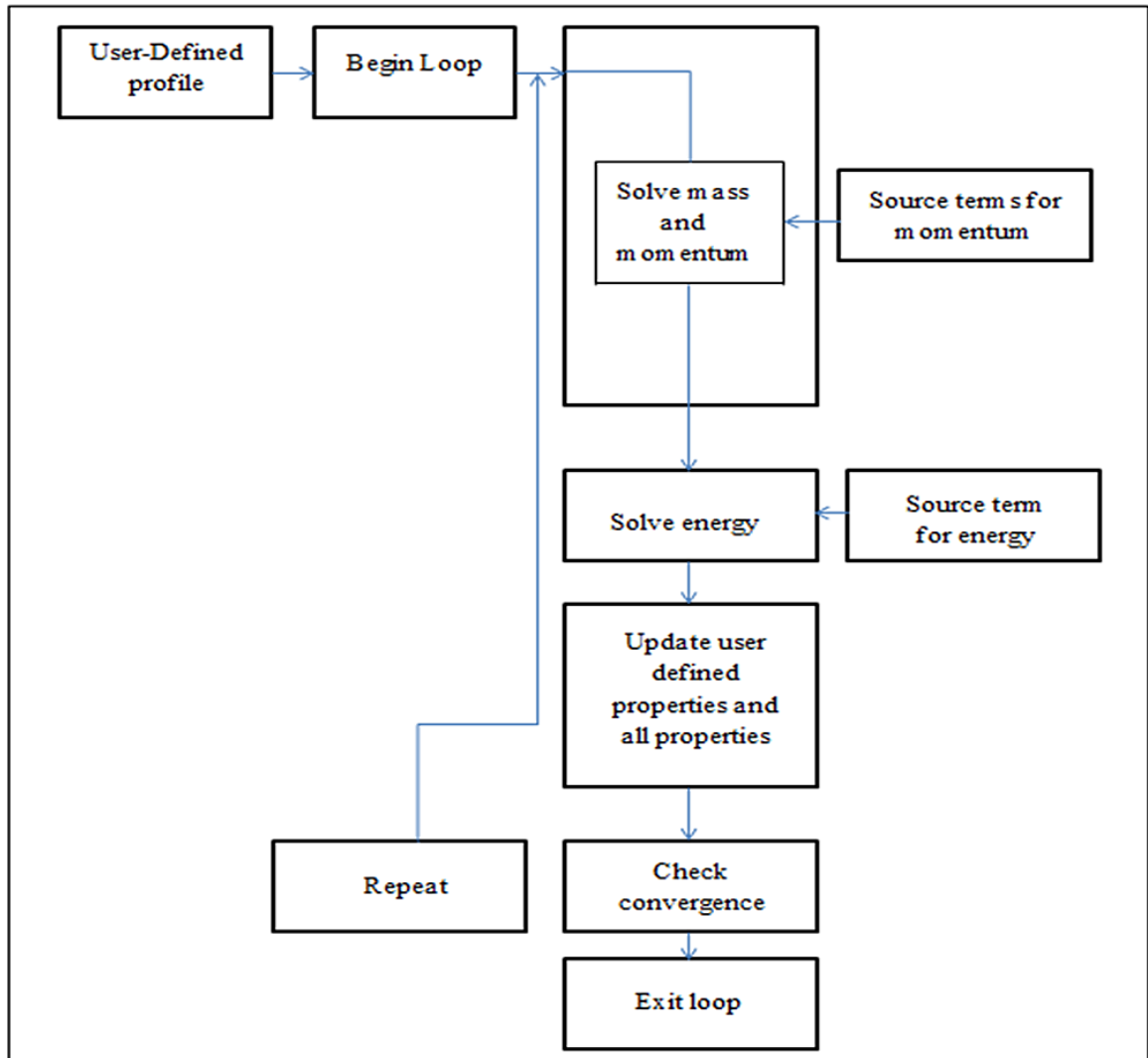
Figure 3.3: Schematic representation of implementation of solution process.

as custom cell zone conditions that varies as a function of spatial co-ordinates and time. The UDF is compiled at the runtime by an in-built complier/interpreter in FLUENT.

Implementation of UDF can be explained as follows. Once the UDF is interpreted, the function is available in the graphical user interface of FLUENT. This UDF is called at every time-step. In this user-defined function, weld center is calculated depending upon the current time. The UDF loops over all the cell faces on the top surface. Inside this loop, the distance between each cell face center and the current weld position is calculated. If this distance is less than or equal to the major/minor axes of double ellipsoidal heat source, heat source is applied to that cell , else convection and radiation loss is applied. When it comes to fluid flow, if the distance is less than or equal to the effective radius of the arc only, the EMF and Buoyancy forces are applied to that cell. Marangoni stresses and surface tension are considered in the graphical user interface by giving the value of temperature coefficient of surface tension.

Once the source terms for momentum and energy equations are taken from the UDF, the next

24

step is to apply the temperature-dependent material properties like thermal conductivity, specific heat and density of the specimen. The solver solves the governing equations and checks for the convergence for every iteration and repeats the above step un till the convergence is reached.

3.5   Model Validation with Experimental Results

3.5.1   Welding Process

The experimental results for model validation are taken from [5]. The gap between both the wires is 12 mm. A constant voltage of 32 V is maintained during the entire process. Two polarities were used namely DCEN and DCEP. Current values were 400A, 500A and 600A while both the wires were 2 mm thick. Current values were 600A, 700A and 800A while both the wires were 3.2 mm thick. The length, width and thickness of the specimen are 300 mm, 200 mm, 22 mm respectively.

Temperature measurement was carried out using a thermocouple at three different locations. For this, two thermocouples which were fixed to the work-piece were used simultaneously. First thermocouple, A1 was placed at the distance of 160 mm from left and at a depth of 5 mm below the center line. Second thermocouple, B1 was placed at the distance of 200 mm from left and at a depth of 7 mm below the center line.

3.5.2   Validation

As mentioned earlier that heat source model proposed in [5] with Flux compensation factor (ϕ) is used in the present investigation. In order to evaluate the effectiveness of the prescribed values of a, b_f, b_r, c and ϕ at different welding conditions, the simulations have been performed for different polarities, different currents, different wire diameters and at different weld locations. It has been observed that at the simulated a, b_f, b_r and c values given in [5], a small modification in ϕ results in very good agreement in predicted and actual cooling time $t_{800-500}$ or ($t_{8/5}$). The cycles are shown from Fig. 3.4 to Fig. 3.14. Fig. 3.15 gives the comparison between actual and predicted $t_{8/5}$. The shown results comprise of the thermal cycle of the points which show peak temperatures more than 800^0C. The modified flux compensation factor (ϕ_m) and the ϕ in [5] are tabulated in the Table 3.2.

Based on the modified ϕ i.e., ϕ_m, the heat and fluid flow model is simulated under different welding conditions. The results are described and discussed in the following chapter.
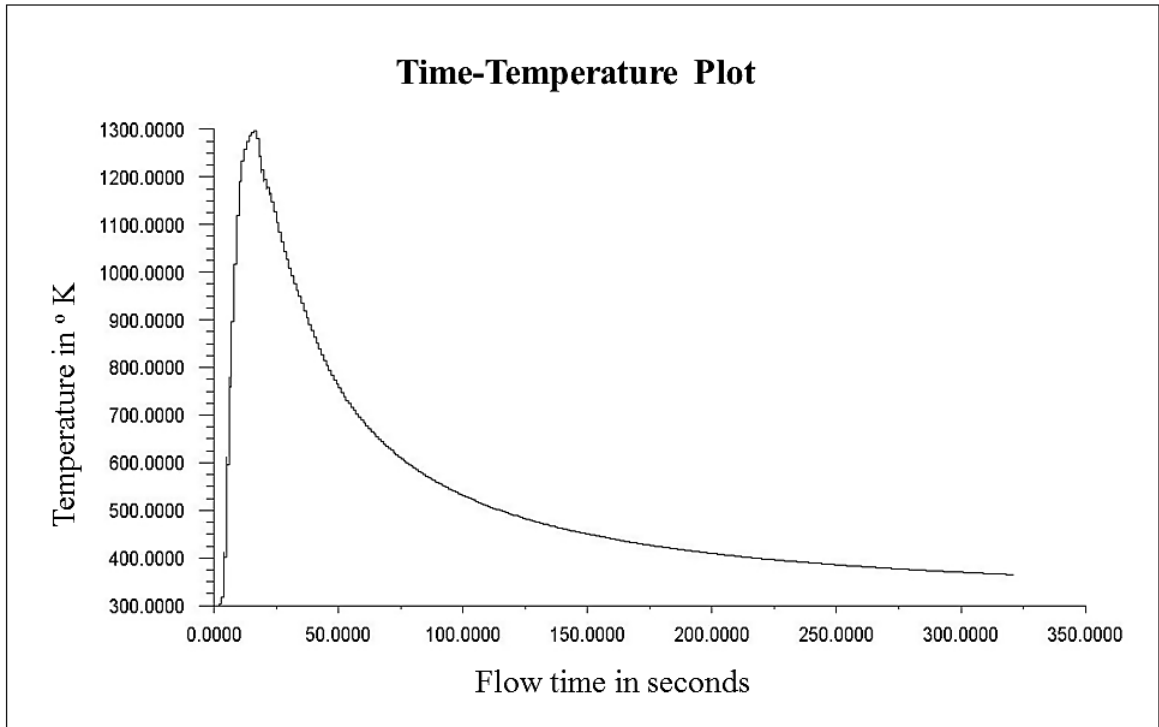
Figure 3.4: Time-temperature plot simulated in FLUENT for 2-2DCEN 500A at point A1
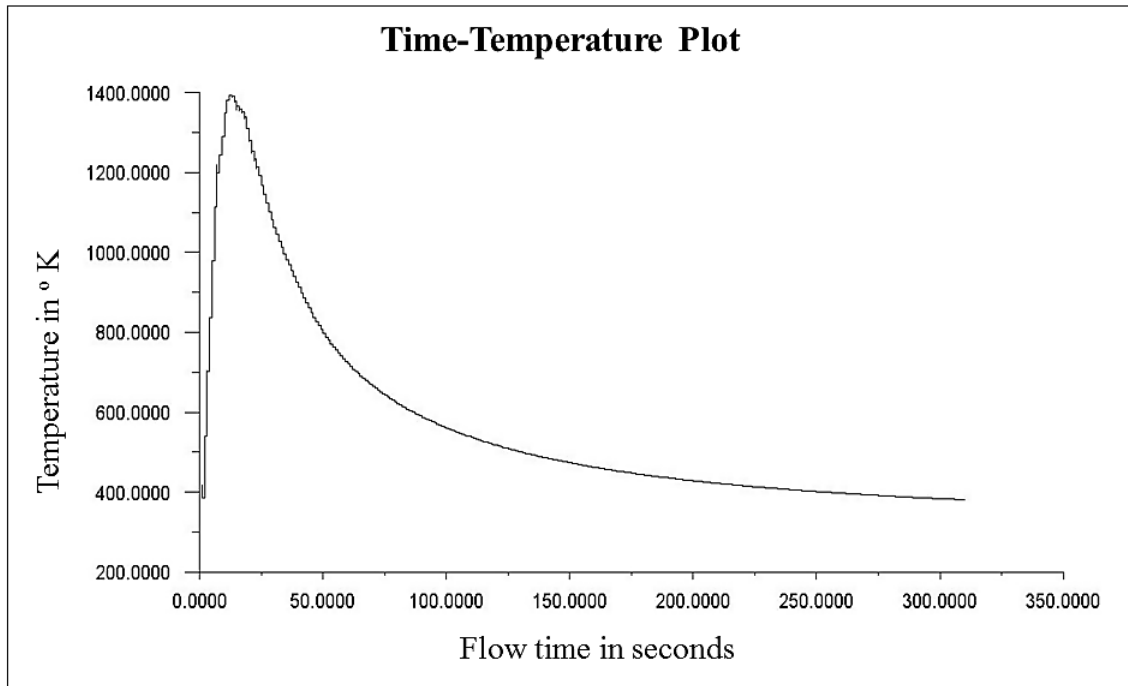

Figure 3.5: Time-temperature plot simulated in FLUENT for 2-2DCEN 600A at point B1
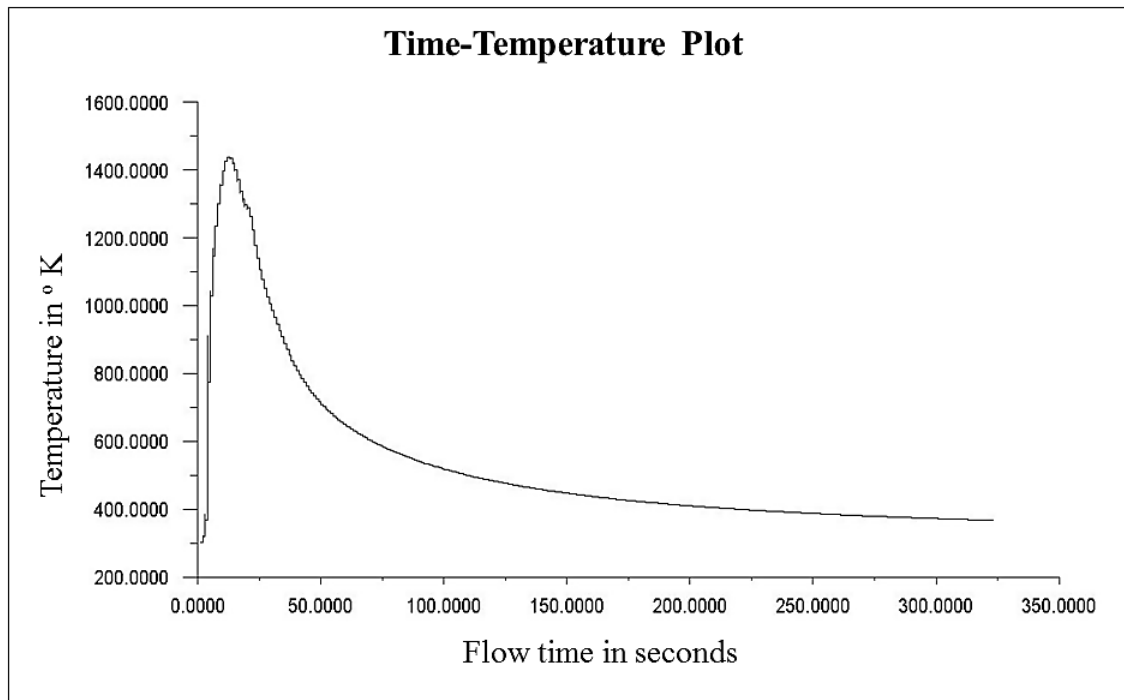
Figure 3.6: Time-temperature plot simulated in FLUENT for 2-2 DCEP 500A at point A1
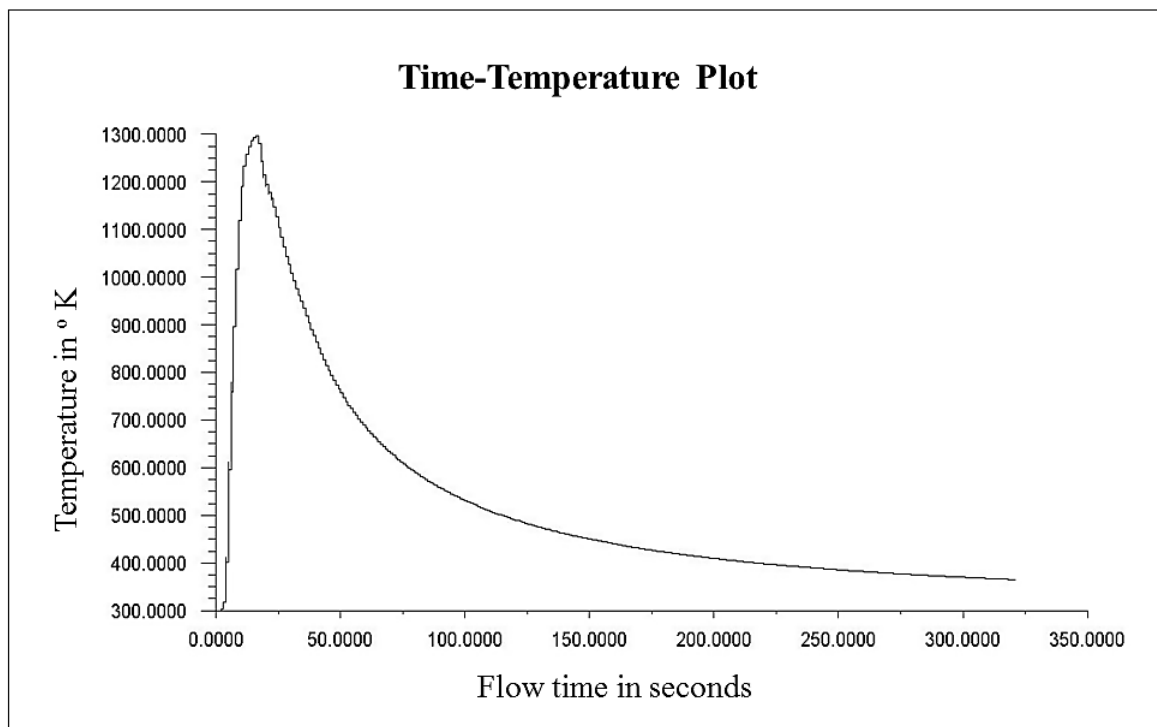

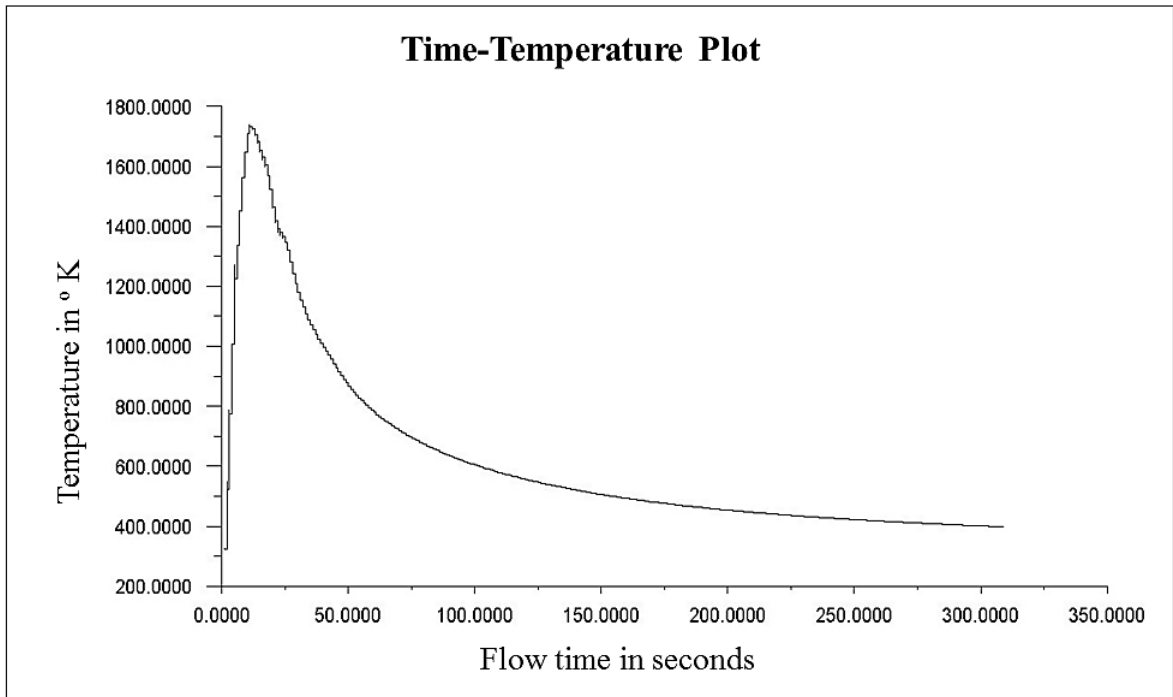Figure 3.7: Time-temperature plot simulated in FLUENT for 2-2 DCEN 500A at point A1

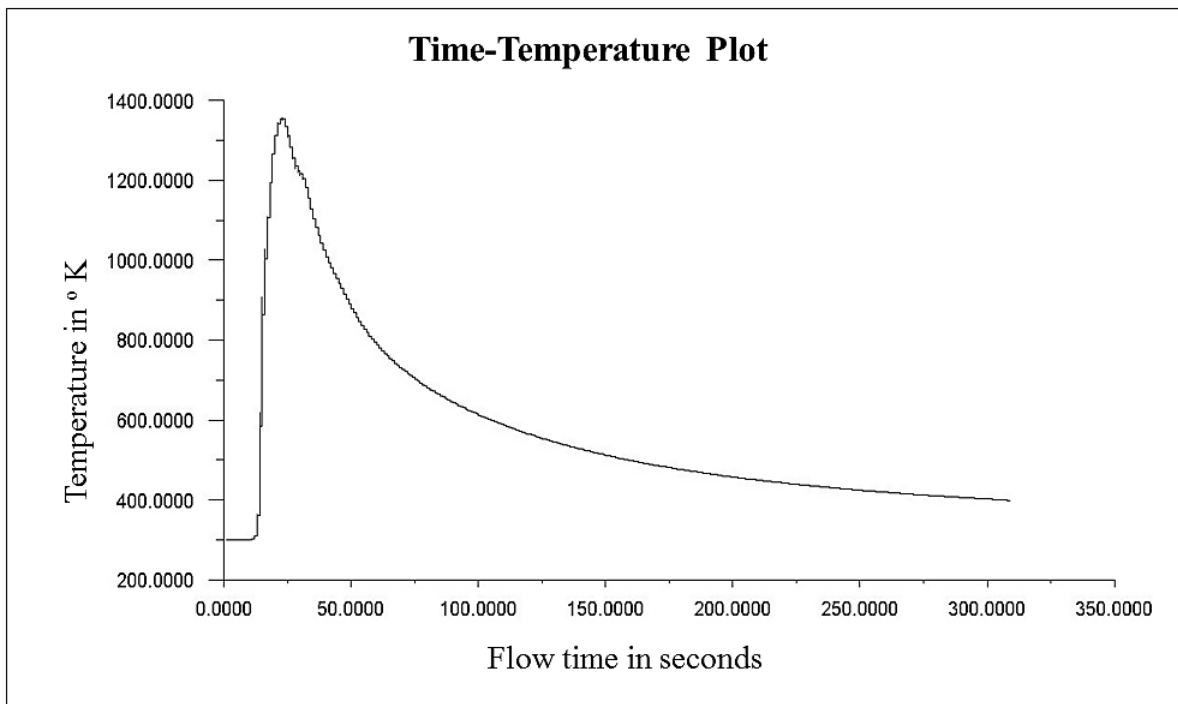Figure 3.8: Time-temperature plot simulated in FLUENT for 2-2 DCEP 600A at point A1

Figure 3.9: Time-temperature plot simulated in FLUENT for 3.2-3.2 DCEN 700A at point A1
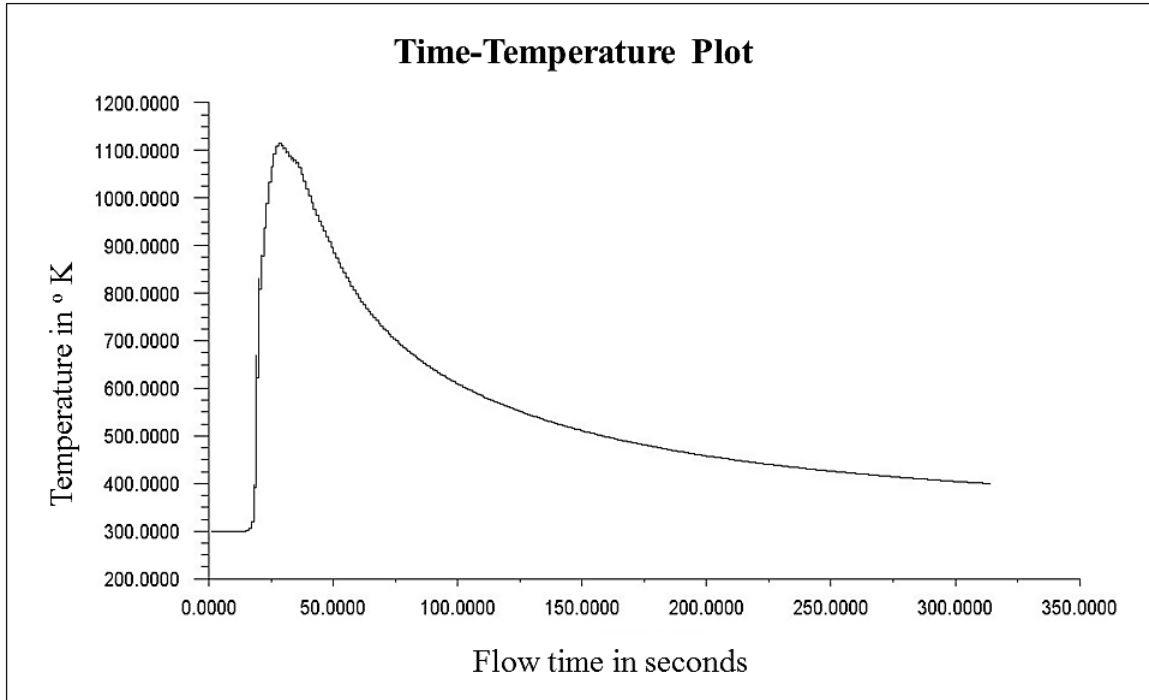
Figure 3.10: Time-temperature plot simulated in FLUENT for 3.2-3.2 DCEN 700A at point B1
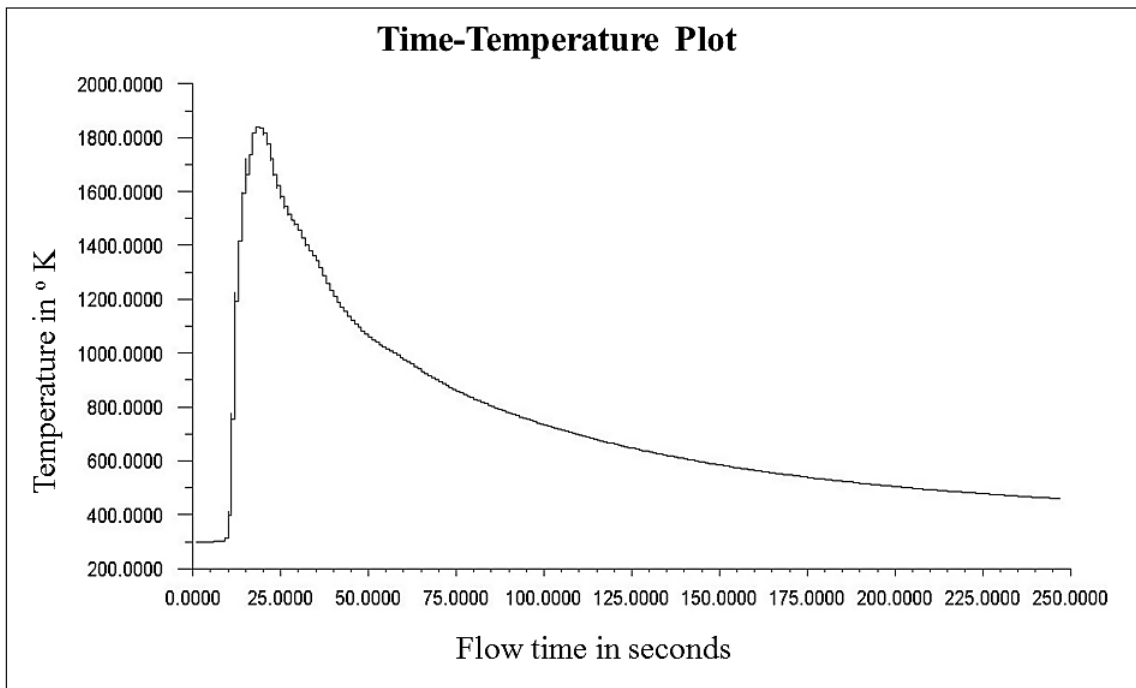

Figure 3.11: Time-temperature plot simulated in FLUENT for 3.2-3.2 DCEN 800A at point A1
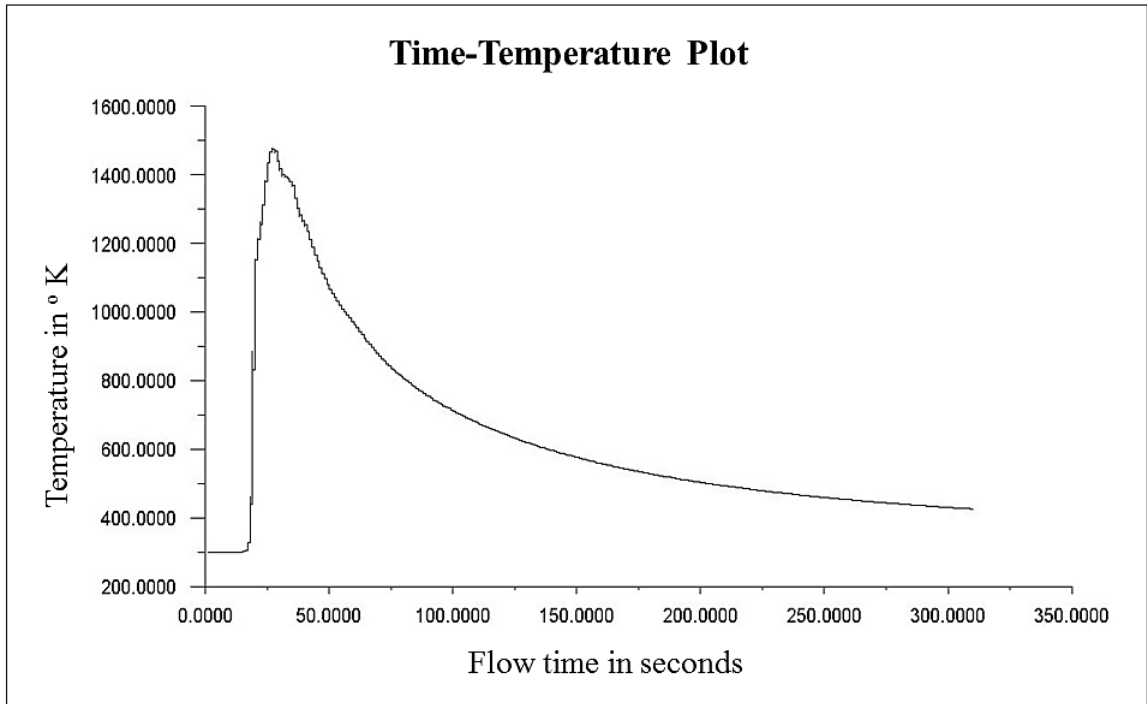
Figure 3.12: Time-temperature plot simulated in FLUENT for 3.2-3.2 DCEN 800A at point B1
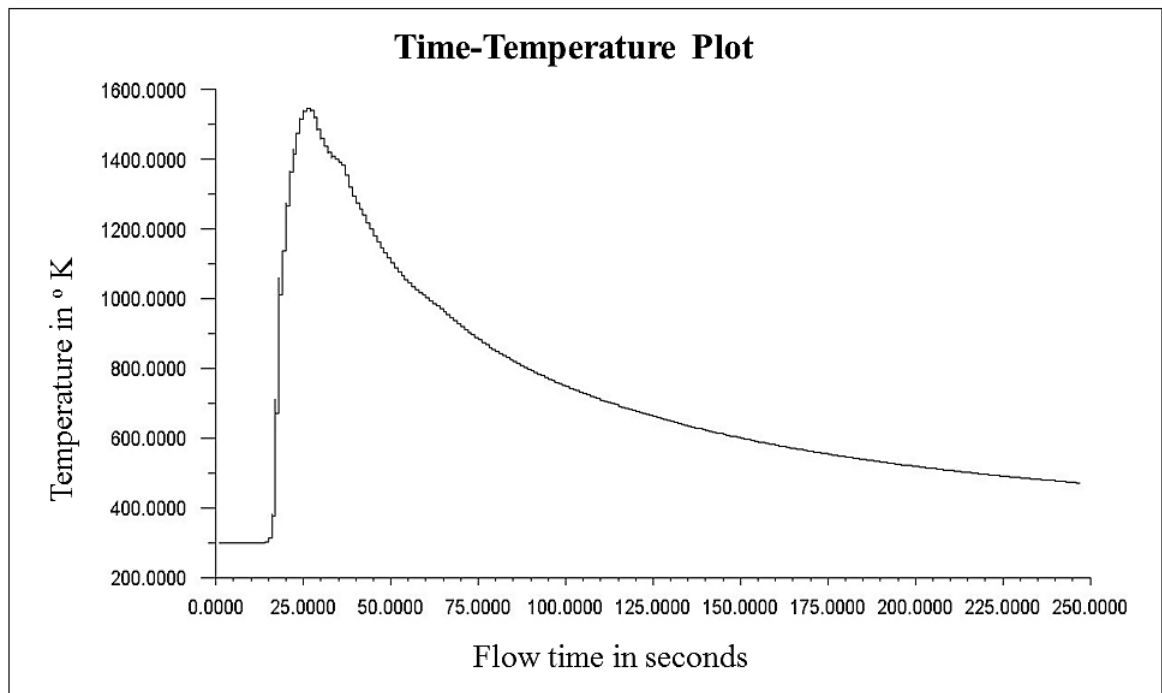

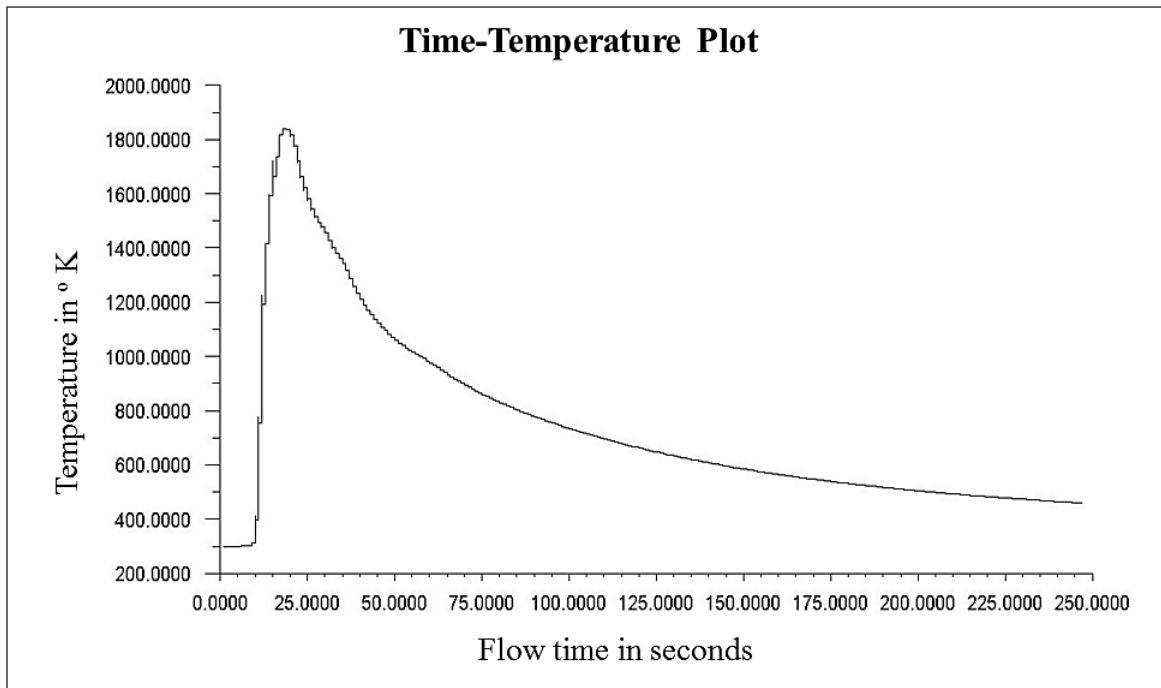Figure 3.13: Time-temperature plot simulated in FLUENT for 3.2-3.2 DCEP 700A at point B1

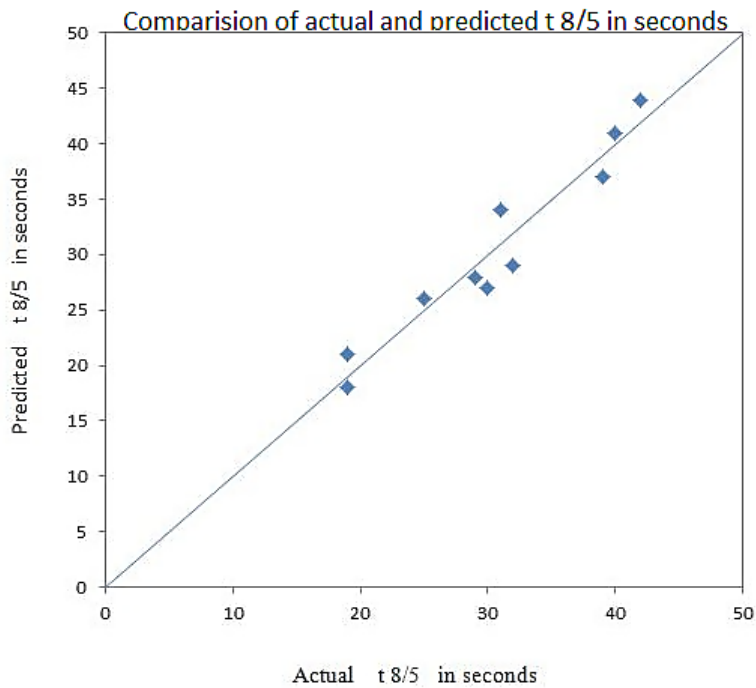Figure 3.14: Time-temperature plot simulated in FLUENT for 3.2-3.2 DCEP 800A at point B1

Figure 3.15: Comparison of actual and predicted t 8/5 in seconds.

Table 3.2: Table showing modified flux compensation factor

S.No	Wire diameter in mm	Polarity	Current in A	ϕ	ϕ_m
1	2-2	DCEN	400	0.380	0.380
2	2-2	DCEN	500	0.510	0.480
3	2-2	DCEN	600	0.600	0.630
4	2-2	DCEP	400	0.600	0.600
5	2-2	DCEP	500	0.650	0.625
6	2-2	DCEP	600	0.720	0.705
7	3.2-3.2	DCEN	600	0.490	0.490
8	3.2-3.2	DCEN	700	0.710	0.720
9	3.2-3.2	DCEN	800	0.770	0.755
10	3.2-3.2	DCEP	600	0.610	0.610
11	3.2-3.2	DCEP	700	0.890	0.910
12	3.2-3.2	DCEP	800	0.930	0.925

Chapter 4

Results and Discussion

An interesting outcome of this research is implementation of heat source parameters obtained from the previous steady-state heat source model [6] into the transient heat source model. In the steady-state heat transfer model the heat source parameters have been obtained through matching the peak temperature. The similar model parameters with little modification in the flux compensation factor results a very good match in the cooling time. The present chapter discusses the effect of process parameter like current, wire-diameter and polarity on temperature distribution, flux compensation factor, fluid flow pattern, magnitude of velocity in the weld pool and the cooling time of the specimen.

4.1 Temperature Distribution

4.1.1 Effect of current on temperature distribution

Figs. 4.1 to 4.6 show the simulated results of temperature contours on the top of the specimen. In the present case 3.2 mm- 3.2 mm wire diameters at 600 A, 700 A and 800 A currents are considered for the study. Each current has been considered at DCEN and DCEP polarities because when the polarities change, the fraction of heat available for the specimen also changes even if the current supplied is same. It is evident from Figs. 4.1. to 4.3 that in the case of DCEN, at lower currents, the expanse of temperature contours in the front direction is significant, where as at higher currents, the expanse of temperature contours in front direction is less significant than in rear direction. This is due to more melting at higher current that results in lesser availability of heat for work-piece melting. However in the later stage the heat of molten metal from the electrode dissipates to the work-piece resulting in more expansion of heat in the rear direction. The same phenomenon also affects the maximum temperature observed in the weld pool, as shown in Fig. 4.7. Lesser maximum temperatures are observed in DCEN compared to DCEP. The maximum temperature in the weld pool is due to the instantaneous interaction of arc with the work-piece. The more amount of molten metal from electrode in DCEN reduces the heat supplied to the work-piece in addition it also hinders the arc from effectively penetrating into the work-piece. In the case of DCEP, as shown in Fig. 4.4 to 4.6 the similar pattern of expansion of heat in front and rear direction with change in the current is observed as in the DCEN. However, higher maximum temperatures are observed in the DCEP because the current supplied to the wire in DCEP is used for melting the work-piece rather than the filler-material. In addition, with the DCEP, the expanse of heat distribution in

the rear direction slightly reduced in comparison to the DCEN. This is due to the well known fact that the DCEP results in deeper penetration allowing heat to conduct in the depth direction more effectively compared to the DCEN.
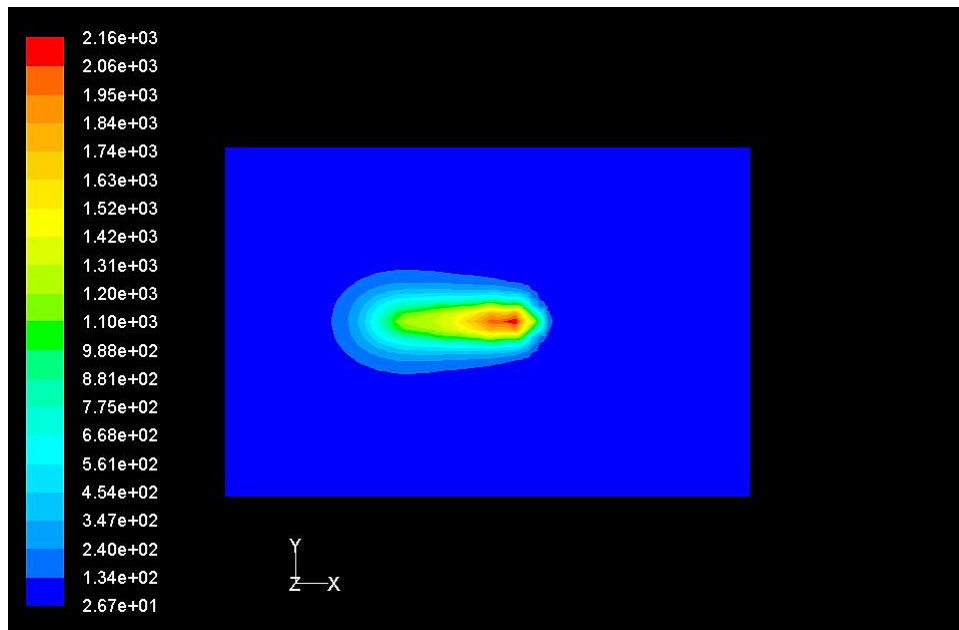

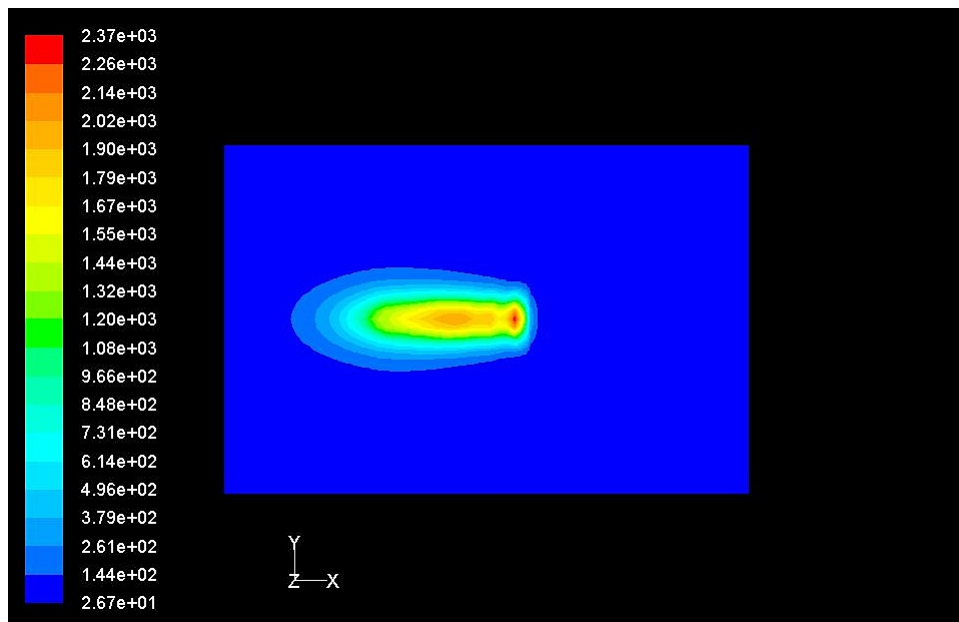Figure 4.1: Numerically simulated temperature contours for 3.2-3.2 DCEN 600A.

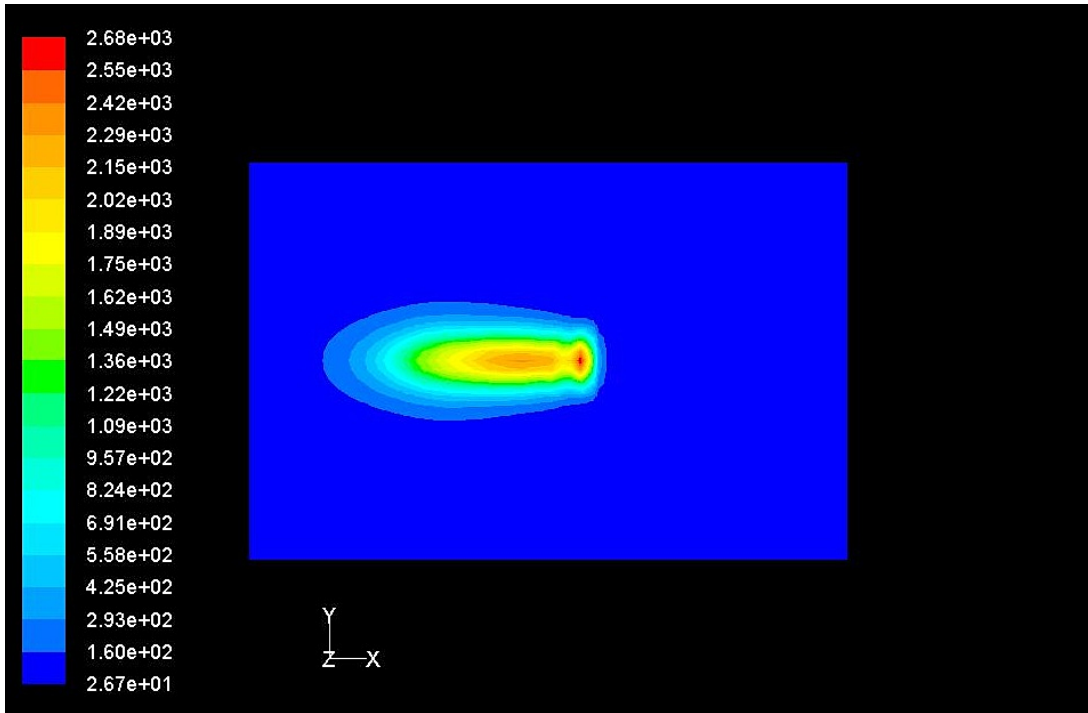Figure 4.2: Numerically simulated temperature contours for 3.2-3.2 DCEN 700A.

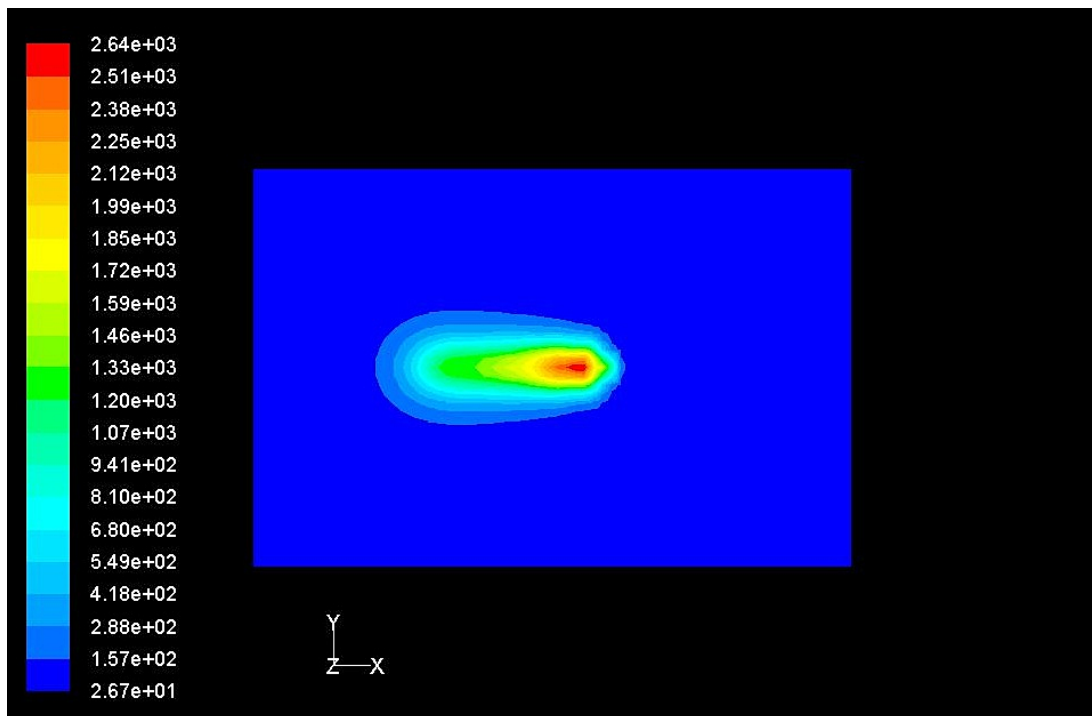Figure 4.3: Numerically simulated temperature contours for 3.2-3.2 DCEN 800A.

Figure 4.4: Numerically simulated temperature contours for 3.2-3.2 DCEP 600A.
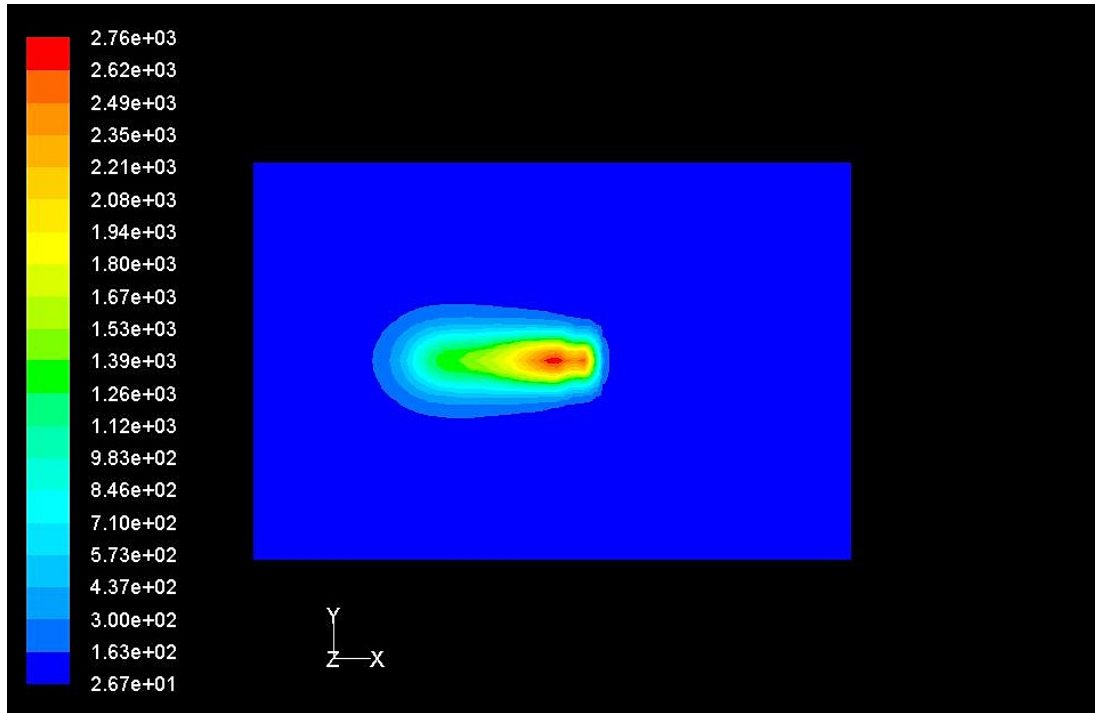
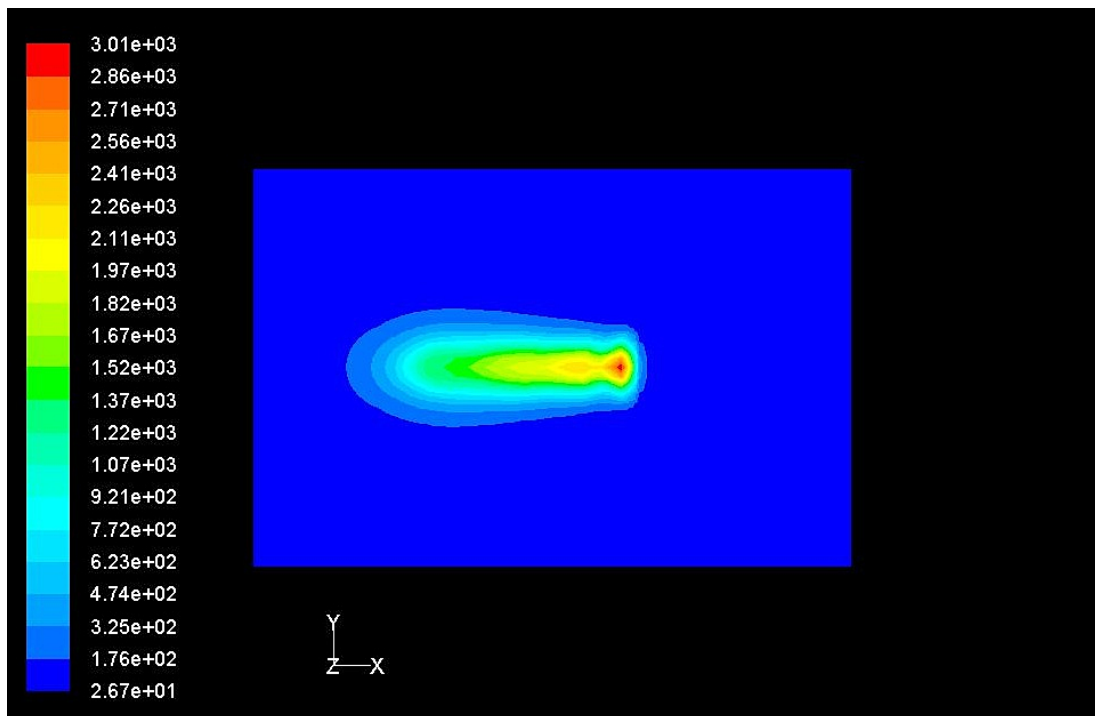Figure 4.5: Numerically simulated temperature contours for 3.2-3.2 DCEP 700A.

Figure 4.6: Numerically simulated temperature contours for 3.2-3.2 DCEP 800A.
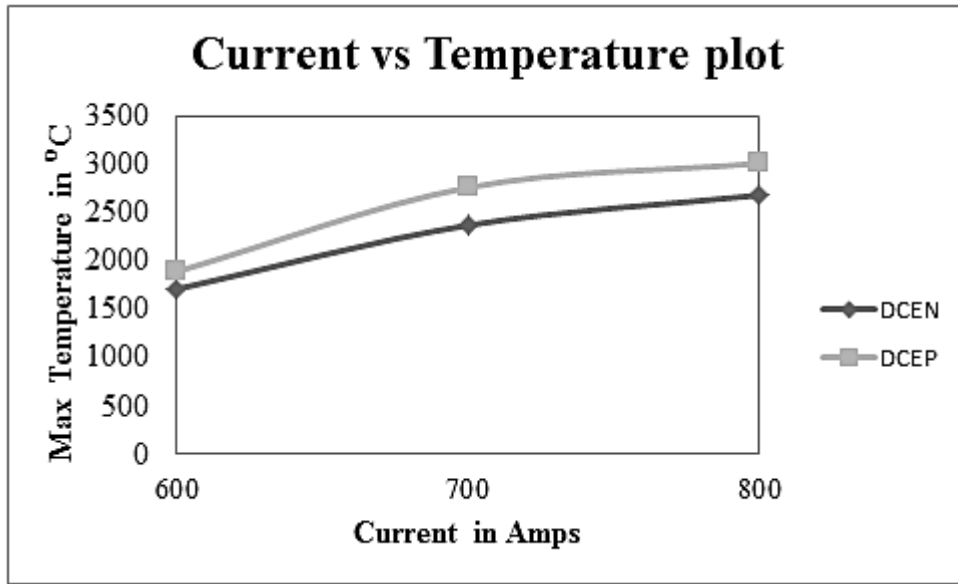
Figure 4.7: Current vs Temperature plot.

4.1.2 Effect of wire-diameter on temperature distribution

The effect of wire diameter can be understood by comparing the temperature contours due to 2-2 DCEN 600A as shown in Fig. 4.8 with the earlier shown temperature contours due to 3.2-3.2 mm DCEN at 600A.
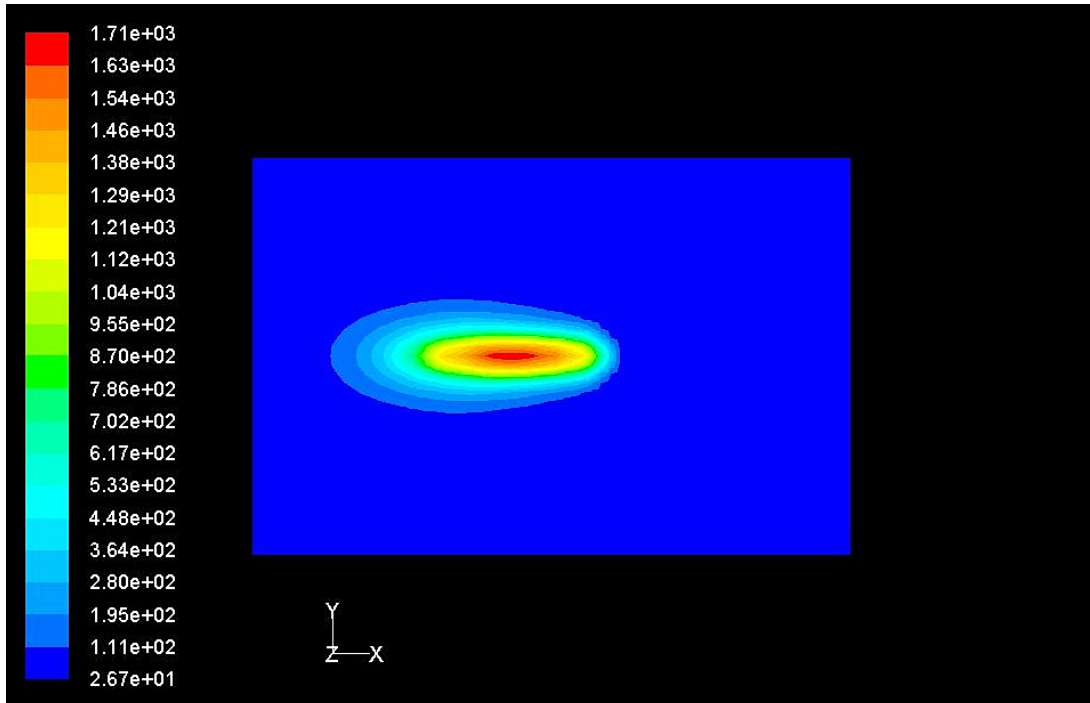

Figure 4.8: Numerically simulated temperature contours for 2-2 DCEN 600A.

In addition, the maximum temperatures in the weld-pool due to different wire diameters at DCEP and DCEN have been compared in the Fig. 4.9. For a given diameter, DCEP gives higher temperature compared to DCEN because more heat is transferred to the work-piece in DCEP. Due to the same reason the rise in the maximum temperature on the specimen is more for larger diameters compared to that of smaller diameters. Melting rate of the wire with lesser diameter is more when compared with that of a wire with more diameter for the same power supply. This melting causes a subsequent melting of flux and filler material. So, the expanse of heat distribution is more on the top layers of the work-piece than along the depth direction. It is important to note that for the same wire diameter the expanse along the transverse and depth directions is more in DCEP. Similarly in DCEN, expanse along the longitudinal direction, in both front and rear directions is more because of more melting of filler material.
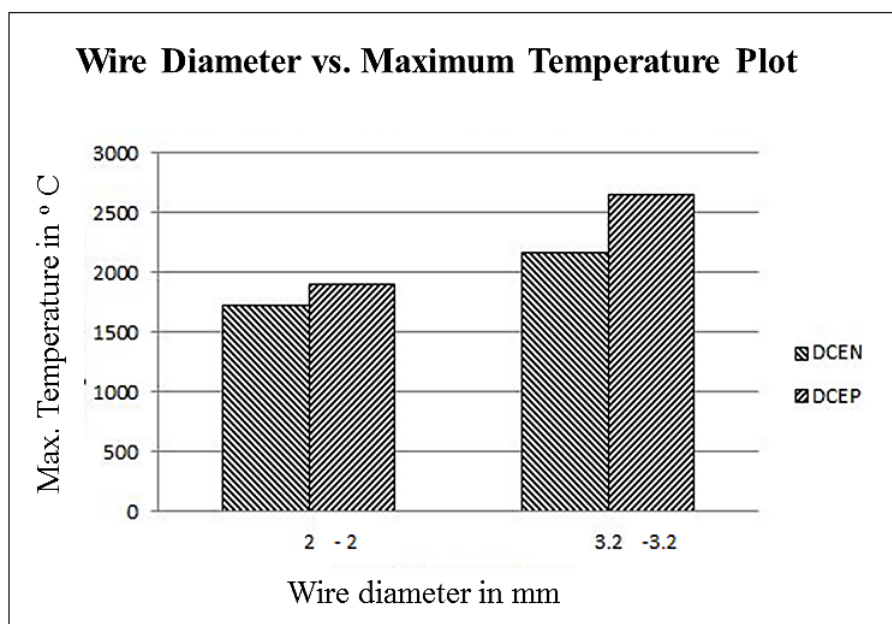
Figure 4.9: Effect of diameter on maximum temperature

4.1.3 Effect of polarity on temperature distribution

An interesting outcome of study of temperature contours along the depth direction is depth of penetration. An idea on depth of penetration can be framed by tracing the expanse of temperature contours along the depth direction as shown in Figs. 4.10 and 4.11. It has been observed that DCEP has deeper penetration where as DCEN has shallower penetration. Fig. 4.12 shows the effect of polarity on depth of penetration. It is clear that for a given polarity, higher the current, higher is the penetration depth. For the same current DCEN has less penetration depth compared to DCEN. The reason can be stated as in DCEP, as the current increases more heat is transferred to the specimen. This heat causes more melting and eventually more fluid flow. Concentration of more fluid in a smaller weld pool invokes digging action. So the penetration depths are higher in DCEP.
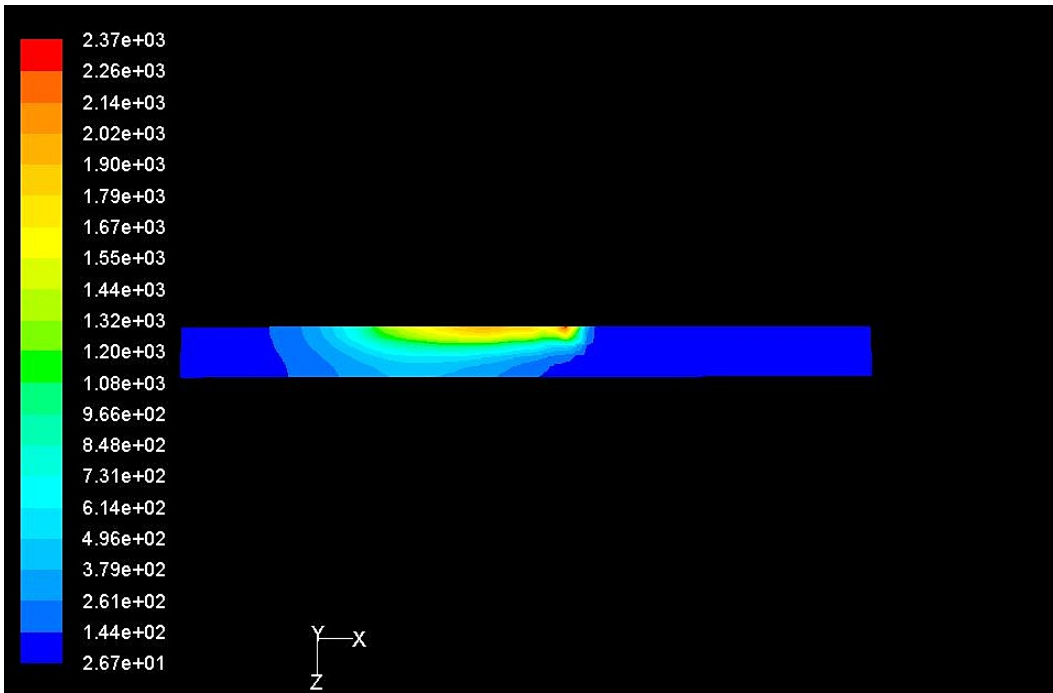
Figure 4.10: Numerically simulated temperature distribution in longitudinal section for 3.2-3.2 DCEN 700A.
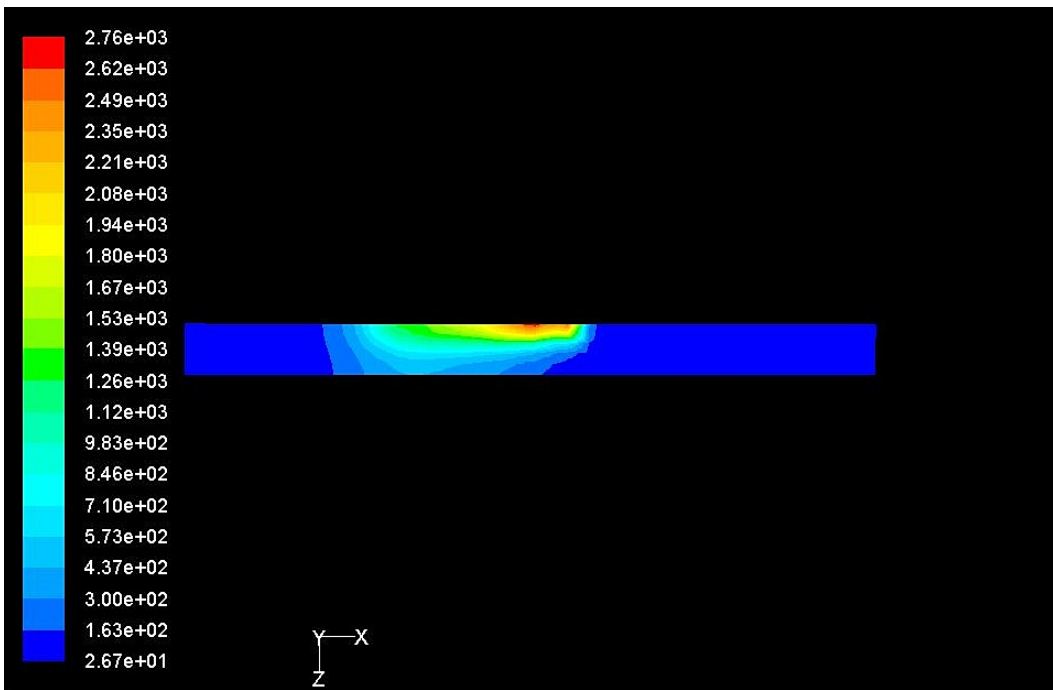

Figure 4.11: Numerically simulated temperature distribution in longitudinal section for 3.2-3.2 DCEP 700A.
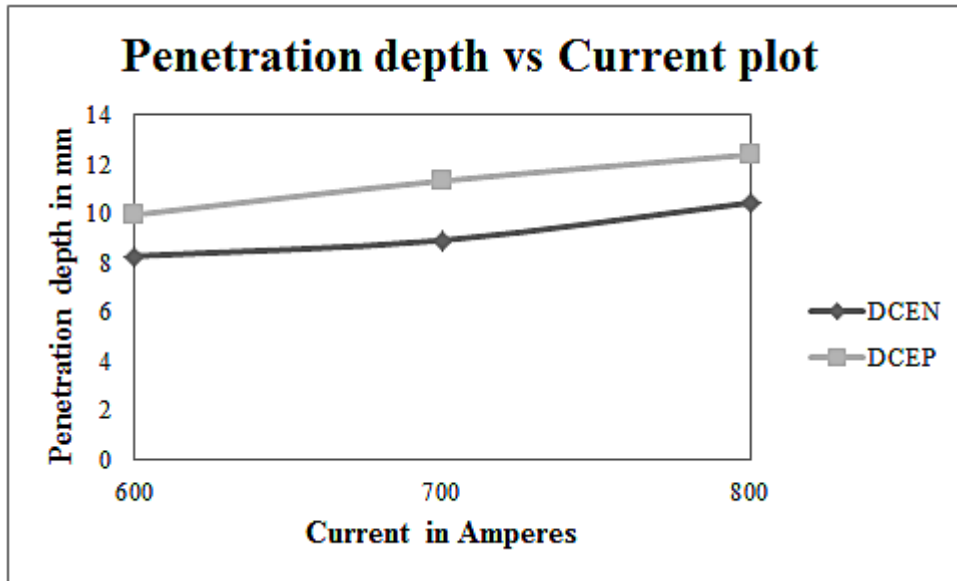
Figure 4.12: Effect of polarity on depth of penetration

4.2 Flux Compensation Factor

Out of the total amount of heat supplied to the work-piece, only a fraction of it is available for the melting of work-piece. The rest of the heat is consumed by flux and filler materials and lost into atmosphere by convection and radiation losses. Flux compensation factor represents the fraction of heat available to melt the work-piece. This section intends to analyze the effect of current, wire-diameter and polarity on flux compensation factor.

4.2.1 Effect of current on flux compensation factor

Fig. 4.13 shows the relationship between current and flux compensation factor at different polarity and wire diameters. Note that flux compensation factor does not have units because it represents the fraction of heat available. Here 5 currents ranging from 400A to 800A with an interval of 100A are considered for the study. It has been observed that as the current increases the fraction of heat available for melting the work-piece also increases. Hence the flux compensation factor also increases with current. Flux compensation factor increases with current irrespective of the polarity. Flux compensation factor is lower in DCEN compared to that of DCEP because more amount of heat is consumed by flux and filler material in DCEN and the fraction of heat available for work-piece is less.

4.2.2 Effect of polarity on flux compensation factor

This study is made on the effect of polarity on the flux compensation factor. In DCEP, the fraction of heat available for melting the flux and filler material is less compared to that of the fraction of heat available for melting the work-piece and vice-versa. So, for all currents, it is observed that DCEP has higher flux compensation factor than DCEN polarity. For DCEN polarity, the trend of
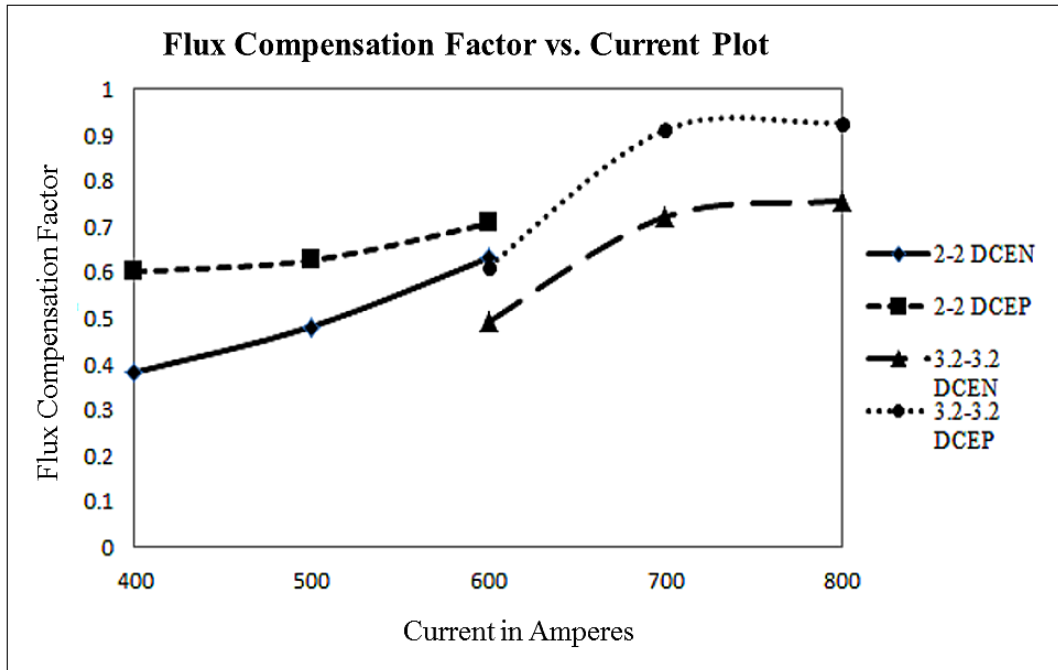
Figure 4.13: Effect of current and polarity on flux compensation factor

increase in the flux compensation factor is gradual with an increase in current. The reason is clear that more the current supplied, more will be the heat available for the specimen to melt. From the studies on effect of polarity on temperature distribution, it is evident that the penetration is less in DCEP. So the scope of digging action does not come into picture even at higher currents. The same case does not seem to hold good in DCEP polarity. In DCEP, the trend of increase in flux compensation factor is gradual at lower currents where as when it comes to higher currents there is a sharp rise in flux compensation factor. The fraction of heat available in this case is used for rising the work-piece to the liquidus temperature in the initial stage. The rest of the heat is used for penetration into the specimen.

4.2.3   Effect of wire-diameter on flux compensation factor

In order to study the effect of wire diameter on flux compensation factor the cases where current of 600 A is supplied from the power source are considered. If the same amount of current is supplied, then the wire with lesser diameter melts quickly compared to that of the wire with larger diameter. Due to this reason more amount of heat is available to the flux which surrounds the electrode molten metal. Hence the flux compensation factor is lower for wires with lesser diameter. However, in case of wire with same diameter, DCEN polarity supplies lesser fraction of heat to the specimen compared to DCEP for all the diameters of the wire because in DCEN polarity the fraction of heat that is used for melting the flux and filler material is more compared to that of the fraction of heat that is supplied to the work-piece.

4.3 Fluid Flow pattern

A significant outcome of the present research is, depicting the fluid flow pattern. Figs. 4.14 and 4.15 show the fluid flow pattern at the top surface where as Figs. 4.16 and 4.17 show the fluid flow pattern in the longitudinal plane. In the figure, positive X-direction shows the direction of welding. Weld pool is formed during the welding process as the wire navigates along positive X-direction because of melting and fluid flow in the work-piece. It is obvious that the front portion of weld pool is still in solid state whereas the rear portion is in molten state. So the fluid hits the solid region and reverses within the weld pool. This pattern can be seen in the Fig.4.14 to Fig.4.17.
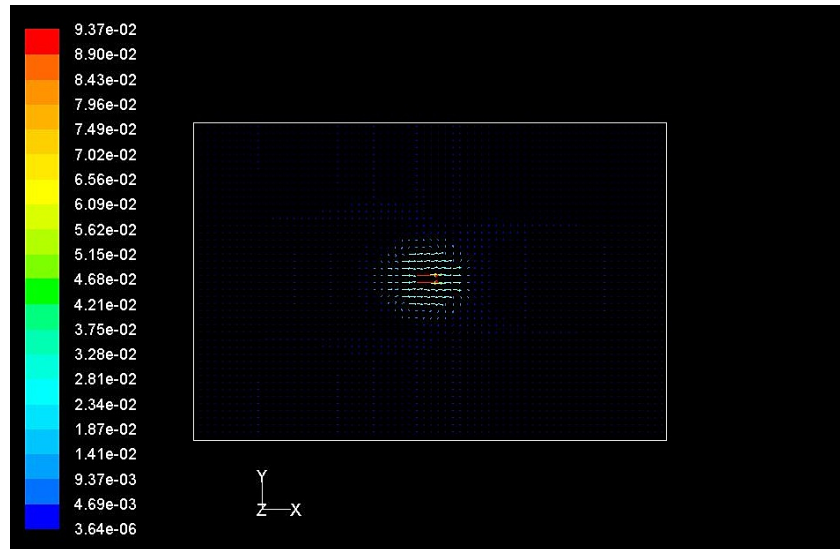

Figure 4.14: Fluid flow pattern during welding on the top surface at 2-2 DCEP 500A.
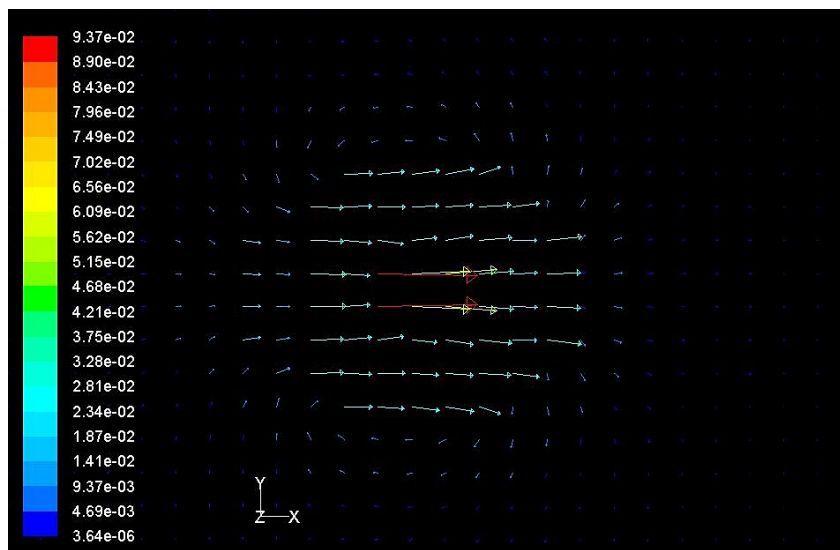

Figure 4.15: Zoomed view of fluid flow pattern on the top surface at 2-2 DCEP 500A.

At the longitudinal plane, fluid flow is directed along the weld direction, i.e. positive X-axis. It hits the unwelded or solid region and reverts back as shown in the figure. The magnitude of velocity vectors is reducing along the depth direction. Magnitude of velocity vectors is more significant upto half of the thickness of the weld plate only. This adds more strength to the fact that fluid flow is taking place within the weld pool only upto the penetration depth.
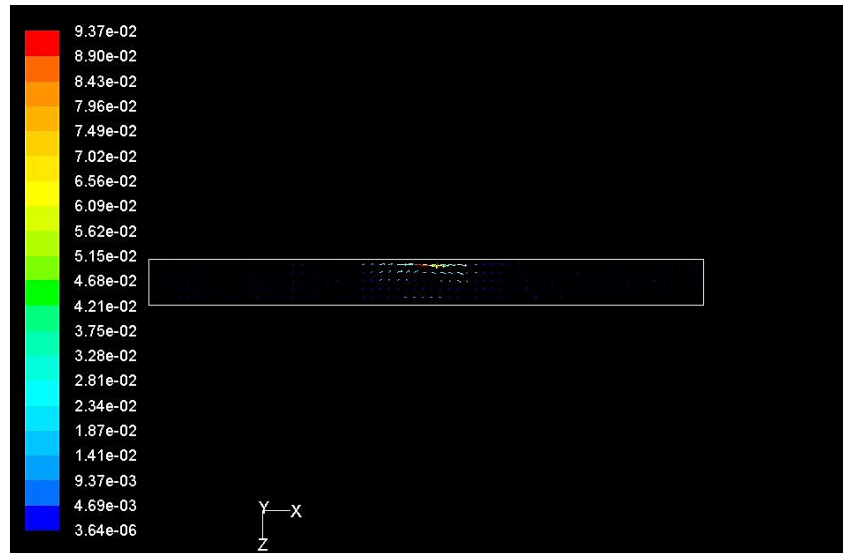

Figure 4.16: Fluid flow pattern in the longitudinal plane at 2-2 DCEP 500A.
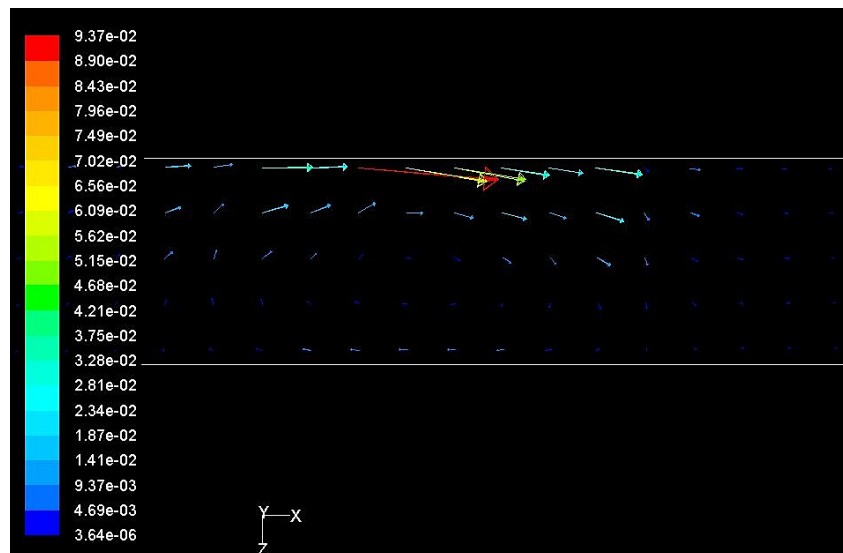

Figure 4.17: Zoomed view of fluid flow pattern in the longitudinal plane at 2-2 DCEP 500A.

4.4 Magnitude of Velocity Vectors

The velocity vectors basically represent the magnitude and direction of displacement of a particle with respect to time. The direction of motion of the molten metal is seen in the previous section. This section deals with the magnitude of velocity vectors and their change with current, diameter and polarity. Velocity gradient exists within the weld pool which enables the fluid flow.

4.4.1 Effect of current on magnitude of velocity vectors

The Fig. 4.18 to Fig. 4.23 depict the velocity vectors at the top surface at different welding conditions followed by figure 4.24 that gives the relationship between welding conditions and the magnitude of minimum and maximum velocities. It is evident that as the current increases, the magnitude of maximum velocity also increases irrespective of the polarity. This increment is more significant in DCEP rather than in DCEN owing to the melting of work-piece and digging action due to fluid flow. At lower currents the magnitude of maximum velocity is observed to be almost similar because of low melting rate even in DCEP. In DCEP, as the current increases, fluid flow rate increases which further causes the increase of magnitude of maximum velocity in the weld pool.
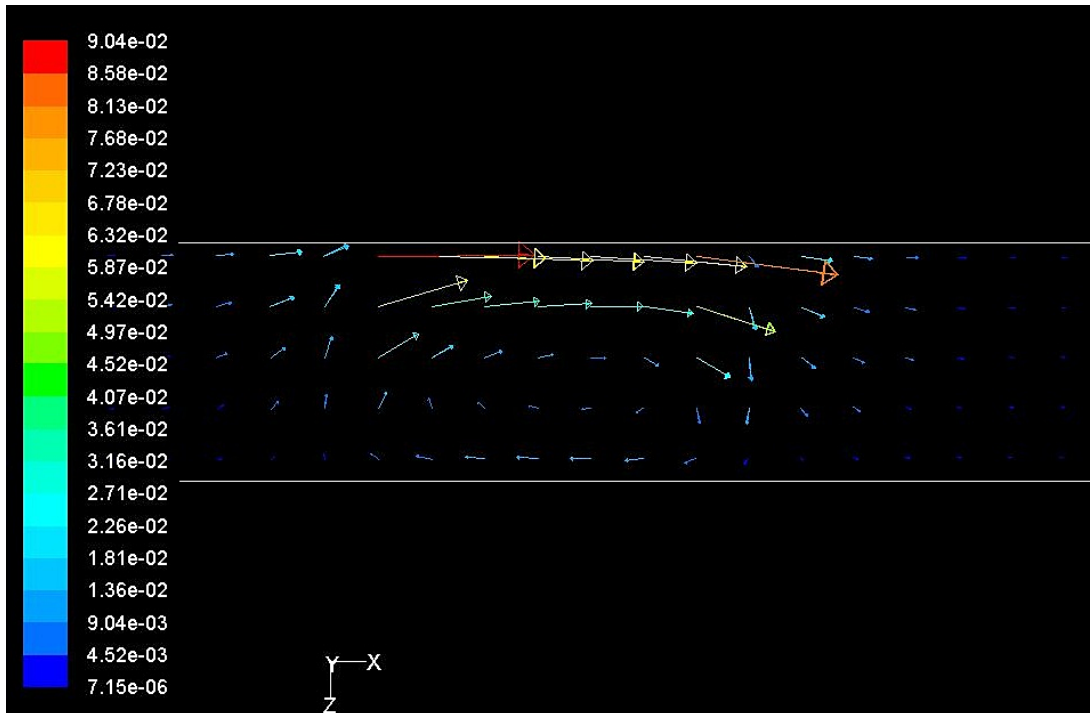
Figure 4.18: Magnitude of velocity vectors for 3.2-3.2 DCEN 600A

4.4.2 Effect of wire-diameter on magnitude of velocity vectors

As shown in Fig. 4.24, for the same wire diameter, DCEP gives higher maximum velocity for all wire-diameters. For a given wire diameter increase in the maximum velocity is more significant at

Figure 4.19: Magnitude of velocity vectors for 3.2-3.2 DCEN 700A

Figure 4.20: Magnitude of velocity vectors for 3.2-3.2 DCEN 800A

Figure 4.21: Magnitude of velocity vectors for 3.2-3.2 DCEP 600A

Figure 4.22: Magnitude of velocity vectors for 3.2-3.2 DCEP 700A

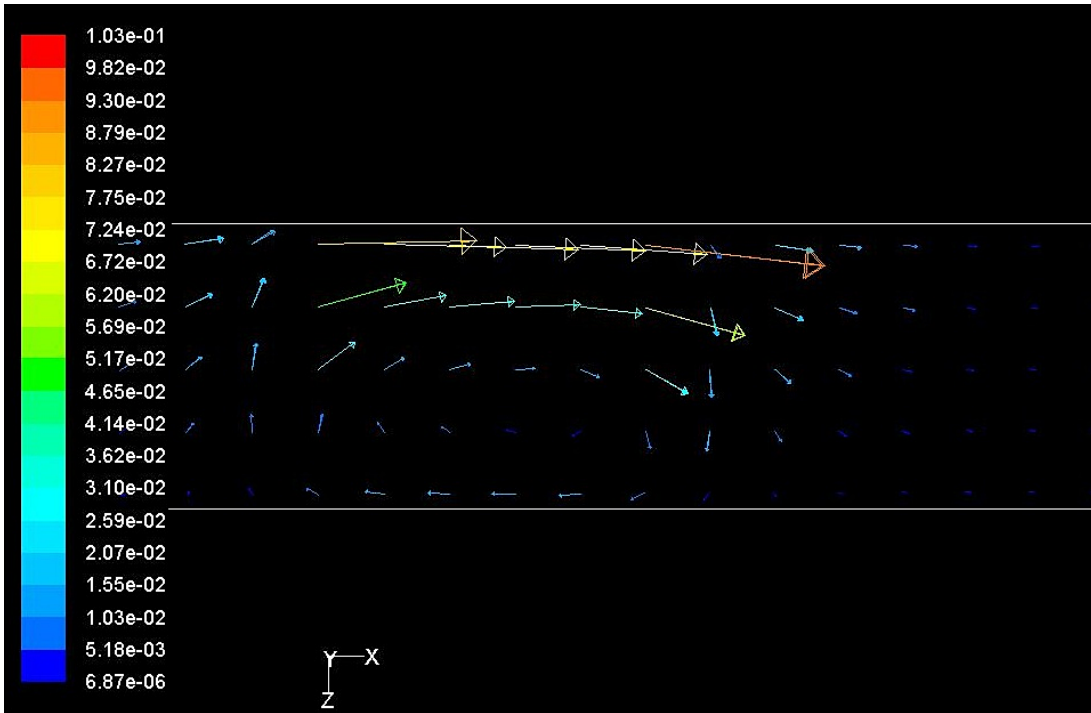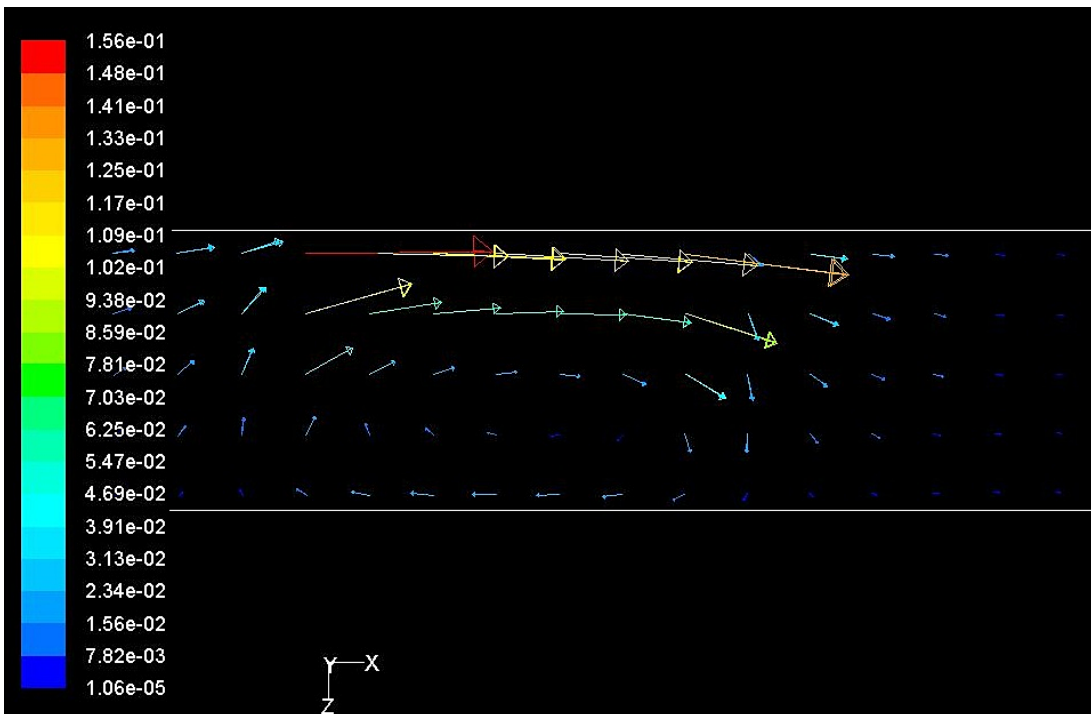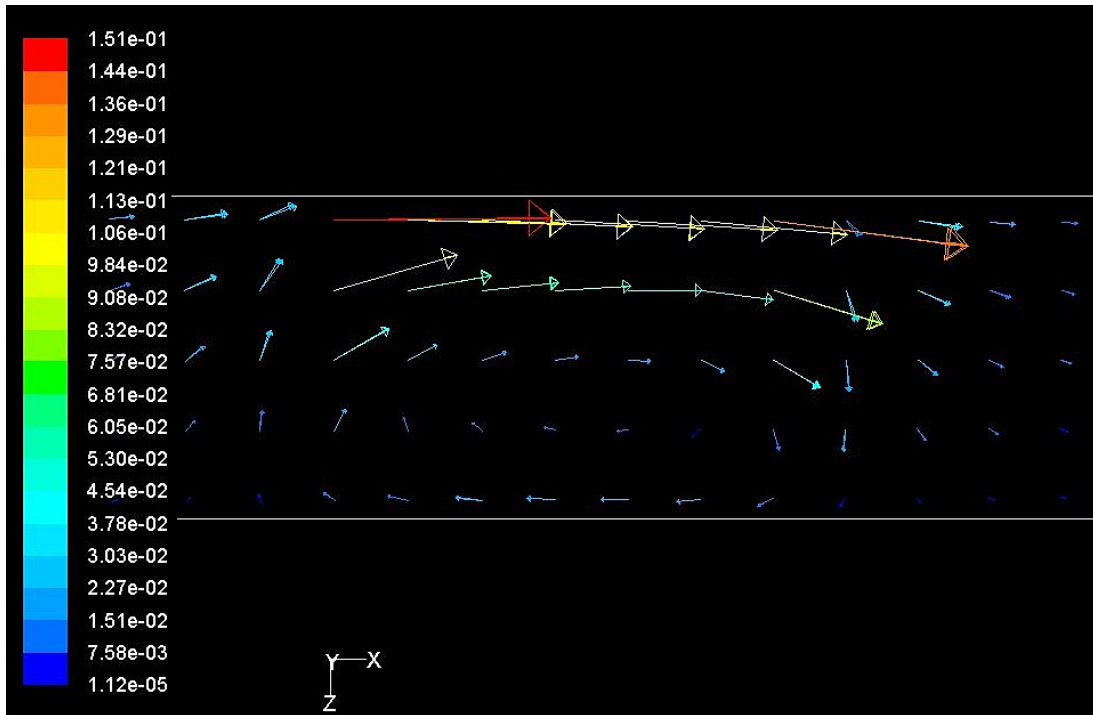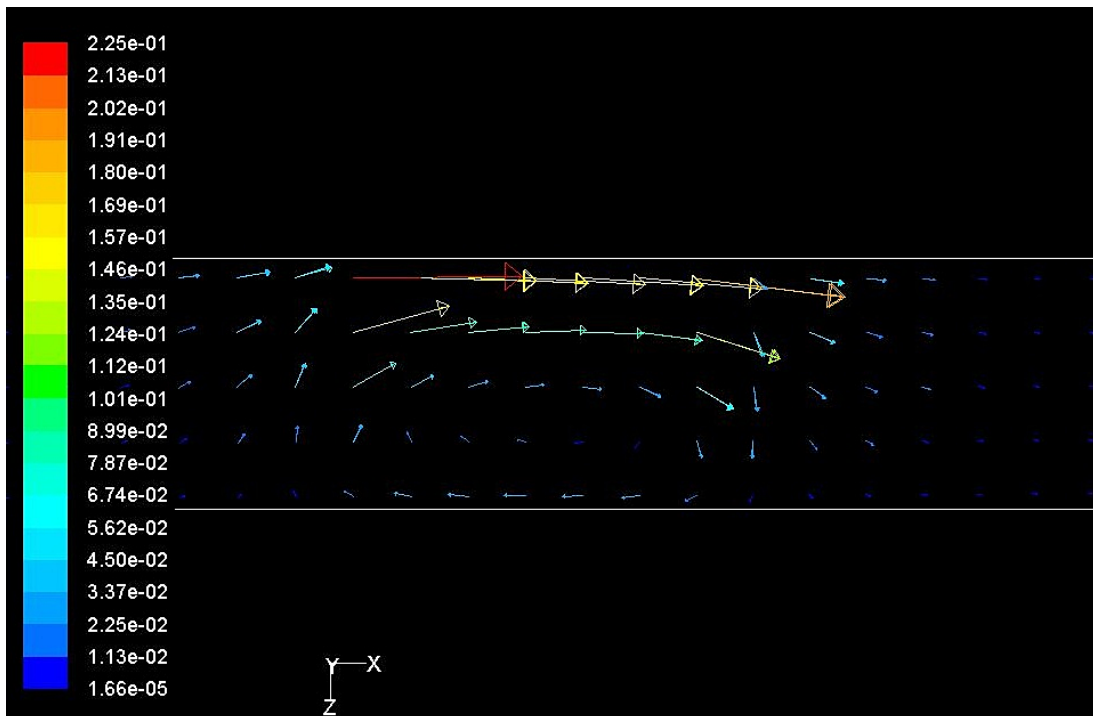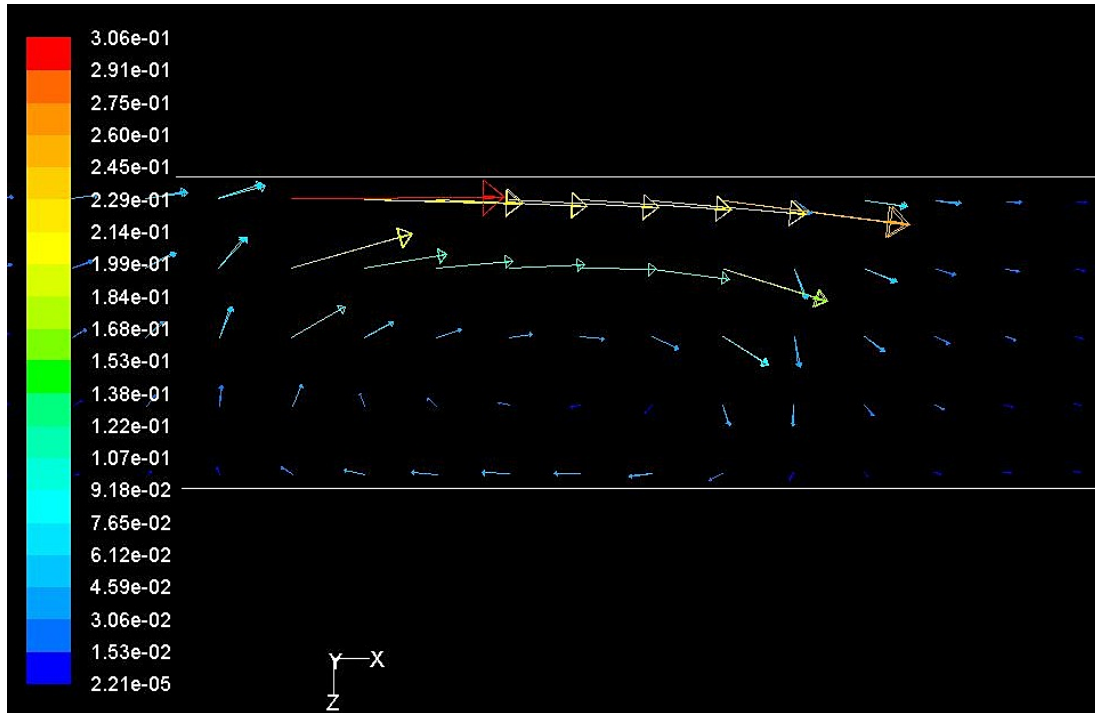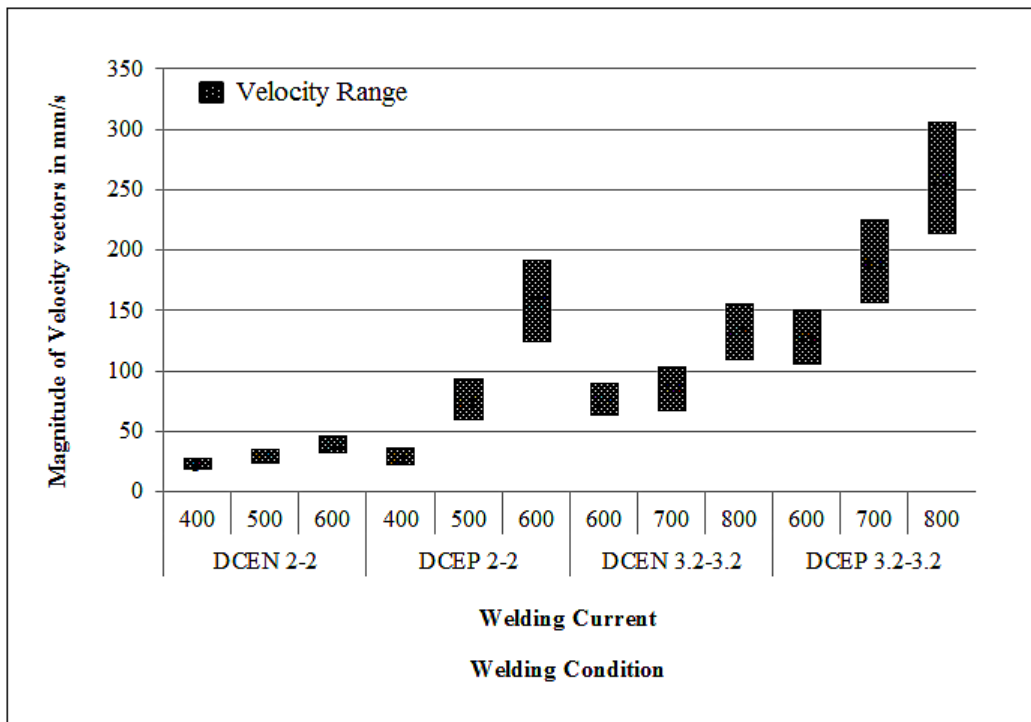Figure 4.23: Magnitude of velocity vectors for 3.2-3.2 DCEP 800A

Figure 4.24: Effect of welding conditions on velocity range.

higher currents rather than at lower currents. This can be a reason for more penetration in DCEP. For the same wire diameter, if the wire is connected to negative terminal, then there is more melting of the wire or filler material than that of work-piece. If the wire is connected to positive terminal, then the melting rate of wire is less. More melting takes place at specimen. This is a reason for higher velocities in DCEP. This reason holds good for both the diameters of the wire.

4.4.3 Effect of polarity on magnitude of velocity vectors:

This effect of polarity on magnitude of velocity vectors within the weld pool is studied with two approaches. First approach deals with the effect of polarity on magnitude of maximum velocity in the weld pool and the second approach deals with the effect of polarity on magnitude of minimum velocity in the weld pool as shown in Fig. 4.24. It has been observed that maximum velocities are higher in DCEP when compared to DCEN, because heat is confined in a smaller and deeper weld pool in DCEP. So more heat is available for unit volume of the cell which further causes higher reduction in fluid viscosity and hence the maximum velocity is higher in DCEP. The velocity of the fluid decreases along the depth direction. The minimum velocity died down completely outside the weld pool and they became completely insignificant outside the weld pool. The minimum significant velocity within the weld pool is considered for this study. Temperatures decrease along the depth direction and hence the viscosity of the fluid increases hence the velocities reduce. At lower currents, reduction is minimum velocity is not so significant. At the higher currents, minimum velocities reduced drastically which creates higher velocity gradients within the weld pool and hence deeper penetration is observed in DCEP.

4.5 Cooling time

Graphical representation of cooling time of the specimen at different currents and polarities is shown in Fig 4.25. This figure is the Time-temperature plot based on modified flux compensation factor. The temperature of the considered point in the specimen rises when the heat is supplied by the arc, when the arc or heat source is directly above it. The considered point in the specimen cools due to convection and radiation when the arc or heat source is moving away from it. The present research concentrates more on the cooling curve.

4.5.1 Effect of current on cooling time

For a given polarity and same wire-diameter, the cooling time of the specimen decreases as the current increases. As, the current increases, the heat supplied to the specimen also increases. So, deeper weld pools are formed resulting in an increment in the penetration depth. Due to this reason, more time is required to cool the specimen and hence the cooling time decreases.

4.5.2 Effect of polarity on cooling time

For a given current, the cooling time in DCEN is higher compared to that of DCEP because the size of the weld pool is more in DCEN. Since the size of the weld pool is more on the top surface and the penetration depths are lesser, more area is exposed to the atmosphere for cooling. This results in higher cooling time in DCEN polarity.
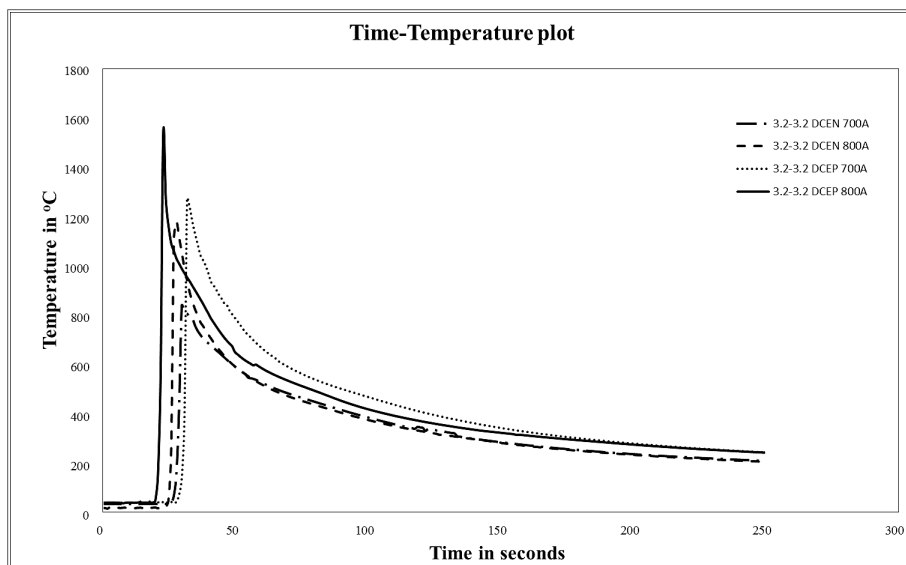
Figure 4.25: Time-temperature plot based on modified flux compensation factor.

Chapter 5

Conclusion

The present modification of twin-wire welding model to a transient cum fluid flow model over the previous model which is a steady state model for heat transfer resulted in the following conclusions:

1. Navier-Stokes equations along with the problem specific initial conditions, boundary conditions and source terms are to be solved to predict the fluid flow phenomenon in twin-wire welding. Obtaining an analytical solution to these equations is highly challenging. So, the complexities were approximated to a solvable state using suitable assumptions and solved using CFD tool. Since CFD is an effective tool to understand the fluid flow and resulting phenomenon in welding, a commercial CFD software AYNSYS-FLUENT is used for performing the numerical analysis.

2. Heat source parameters obtained by considering static heat source in the previous investigation [5] holds good in the transient analysis of moving heat source parameters. However, the previous model could predict the peak temperatures very well but when it comes to predicting the cooling time an average percentage error of 20 percent was observed. In this scenario, a need for modifying the model has been identified. The amount of heat convected in the weld pool plays in important role in the cooling time. As the present model incorporates convective heat flow, an impact was observed on the quantification of heat supplied to the work-piece in form of flux compensation factor. A small modification in the flux compensation factor yields a very good agreement between the predicted and actual cooling time.

3. The role of welding parameters like current, wire-diameter and polarity on temperature of the specimen can be concluded as follows. As the current supplied to the specimen increases, the temperature of the specimen rises irrespective of the polarity. Higher the wire-diameter, more will be the temperature of the work-piece. Higher temperatures of the specimen were seen with DCEP polarity irrespective of the current and vice-versa.

4. The role of welding parameters on flux compensation factor can be stated as follows. For a given polarity, as the current increases, the fraction of heat available for the specimen also increases. So, the flux compensation factor also increases. In general, more the wire-diameter, more is the flux compensation factor. For a given current and wire-diameter, flux compensation factor is more with DCEP polarity and vice-versa.

5. The role of welding parameters on velocity of fluid flow in the weld-pool can be concluded as follows. As the current supplied to the specimen increases, the velocity of the fluid increases because more heat is supplied to the specimen. Higher velocities were observed when the heat is supplied to the specimen using the wire of more diameter whereas for a given wire-diameter higher velocities were seen with DCEP polarity.

6. The role of welding parameters like current and polarity on cooling time can be stated as follows. Cooling time of the specimen decreases as the current supplied to it increases irrespective of the wire-diameter. Since the weld pool size on the top surface are large in and the penetration depths are shallower in DCEN, cooling time is higher with DCEN polarity.

5.1   Scope of Future Work

The present model which describes heat and fluid flow modeling in twin-wire welding can be further improved as follows:

1. In the present investigation, the fluid flow model that is used is a work-piece based model. The effect of pressure due to arc and droplet impingement may be modeled.

2. The electro-magnetic properties of the specimen are considered to be temperature- independent in this research. In the future model, temperature dependent electro-magnetic properties may be incorporated.

3. Studies can be made on the effect of process parameter like current, wire-diameter and polarity on heat affected zone.

References

[1] D. Rosenthal. The Theory of Moving Source of Heat and its Application to Metal Treatments. *Transaction of ASME* 68, (1946) 849–866.

[2] J. Goldak, A. Chakravarthi, and M. Bibby. A New Finite Element Model for Welding Heat Sources. *Metallurgical and Materials Transactions* 15B, (1984) 299–305.

[3] L. Robert. A New Technique for 3-Dimenssional Transient Heat Transfer Computations of Autogeneous Arc Welding. *Metallurgical Transactions* B 21, (1990) 1033–1047.

[4] N. T. Nguyen, A. Ohta, K. Matsuoka, N. Suzuki, and Y. Meada. Analytical Solution of Transient Temperature in Semi-Infinite Body Subjected to Moving Heat Source. *Welding Journal* 78, (1999) 265–274.

[5] A. Sharma, A. K. Chaudhary, N. Arora, and B. K. Mishra. Estimation of heat source model parameters for twin-wire submerged arc welding. *Int J Adv Manuf Technol* 45, (2009) 87 – 97.

[6] A. Sharma, A. Navneet, and S. R. Gupta. Investigation into Arc Behavior during Twin-Wire Submerged Arc Welding. *Materials and manufacturing process* 25:8, (2010) 873–879.

[7] A. P. Mackwood and R. C. Crafer. Thermal modelling of laser welding and related processes: a literature review. *Optics and Laser Technology* 37, (2005) 99 – 115.

[8] D. T. Swift-Hook and A. E. F. Gick. Penetration welding with lasers., volume 54. Weld Res Suppl, 1973.

[9] K. A. Bunting and G. CornDeld. Toward a general theory of cutting: a relationship between the incident power density and the cut speed. *Trans ASME J Heat Transfer* 97, (1975) 116 – 122.

[10] W. ONeill and W. Steen. Review of mathematical models of laser cutting of steel. *Laser Engg.* 3, (1994) 281 – 299.

[11] V. Pavelic, R. Tanbakuchi, O. A. Uyehara, and P. S. Myers. Experimental and computed temperature histories in gas tungsten-arc welding of thin plates. *Welding Journal* 48(7), (1969) 295–305.

[12] Friedman and Glickstein. An Investigation of the Thermal Response of Stationary Gas Tungsten Arc Welds. *Welding Journal* 55, (1976) 408–420.

[13] N. Christensen, V. L. Davies, and K. Gjermundsen. Distribution of Temperature in Arc Welding. *British Welding Journal* 12, (1965) 54–75.

[14] C. R. Heiple and F. E. G. Burgardt, P Rocky. Welding Brazing and Soldering, volume 6. ASM International, 1993.

[15] J. F. Lancaster. The physics of welding. International Institute of Welding, Pergamon press, Oxford, 1984.

[16] A. Kumar and T. Debroy. Calculation of three-dimensional electromagnetic force field during arc welding (2003). *Journal of applied Physics* 94.

[17] C. S. Wu, M. Ushio, and M. Tanaka. Analysis of the TIG welding arc behavior. *Computational Materials science* 7, (1997) 308 – 314.

[18] M. Tanaka, T. Shimizu, T. Terasaki, M. Ushio, F. Koshiishi, and C. L. Yang. Effects of activating flux on arc phenomena in gas tungsten arc welding (2000). *Science and Technology of Welding and Joining* 5, (2000) 397 – 402.

[19] W. Dong, S. Lu, D. Li, and Y. Li. Modeling of the Weld Shape Development During the Autogenous Welding Process by Coupling Welding Arc with Weld Pool. *Journal of Materials Engineering and Performance* 19, (2009) 942 – 950.

[20] Y. Wang and H. L. Tsai. Impingement of filler droplets and weld pool dynamics during gas metal arc welding process. *International Journal of Heat and Mass Transfer* 44, (2000) 2067 – 2080.

[21] M. Tanaka, H. Terasaki, M. Ushio, and J. J. Lowke. A unified numerical modeling of stationary tungsten-inert-gas welding process . *Metallurgical and Materials Transactions A* 33, (2002) 2043 – 2052.

[22] H. G. Fan and R. Kovacevic. A unified model of transport phenomena in gas metal arc welding including electrode, arc plasma and molten pool. *Journal of Physics D, Applied Physics* 37, (2004) 2531–2532.

[23] J. W. Macqueene. Numerical Methods and Measurement Related to Welding Processes Numerical Methods in Thermal Problems , volume 5. Pineridge Press, UK, 1987.

[24] N. L. Arora, G. Biswas, V. Eswaran, K. Muralidhar, T. K. Senguptha, A. Sharma, and T. Sundararajan. Computational Fluid Flow and Heat Transfer. Narosa Publishing House pvt. ltd., 2009.

[25] V. Pavelic. Welding Hand Book, volume 2. 1980.

[26] Kurtz and Segerlind. Finite Element Analysis of Welded Structure. *Welding Journal* 57(7), (1978) 211s–216s.

[27] P. Tekriwal and J. Mazumdar. Finite Element analysis of Three Dimensional Transient Heat Transfer In GMA Welding. *Welding Journal* 150s–156s.

[28] E. A. Bonifaz. Finite Element Analysis of Heat Flow In Single-Pass Arc Welds. *Welding Journal* 59, (2000) 121–125.

[29] S. Prasad and S. Narayanan. Finite element analysis of temperature distribution during arc welding using adaptive grid technique. *Welding Journal* 123–128.

[30] L. Han and F. W. Liou. Numerical investigation of the influence of laser beam mode on melt pool. *International Journal of Heat and Mass Transfer* 4385–4402.

[31] J. Zohu, H. L. Tsai, and P. C. Wang. Transport Phenomena and Keyhole Dynamics during Pulsed Laser Welding. *Journal of heat transfer* 128, (2006) 680–690.

[32] H. Wang, Y. Shi, and S. Gong. Effect of pressure gradient driven convection in the molten pool during the deep penetration laser welding. *Journal of Materials Processing Technology* 184, (2006) 386–392.

[33] H. Wang, Y. Shi, S. Gong, and A. Duian. Effect of assist gas flow on the gas shielding during laser deep penetration welding. *Journal of Materials Processing Technology* 184, (2007) 379–385.

[34] K. C. Tsao and C. S. Wu. *Welding Journal* 67, (1988) 70 – 75s.

[35] M. R. Frewin and D. A. Scott. Finite Element Model of Pulsed Laser Welding (1999). *Welding Research Supplement* 17s.